TEKTONIKA

Cenozoic Relative Movements of Greenland and North America by Closure of the North Atlantic-Arctic Plate Circuit: The Labrador Sea, Davis Strait, Baffin Bay, and Eurekan Orogen

Annabel Causer [1], **Graeme Eagles** *[2], **Lucía Pérez-Díaz** [3], **Jürgen Adam** [1]

[1]Earth Sciences Department, Royal Holloway University of London, Egham, TW20 0EX, United Kingdom | [2]Alfred Wegener Institut, Helmholtz Zentrum für Polar und Meeresforschung, Bremerhaven, Germany | [3]Department of Earth Sciences, Oxford University, Oxford, OX1 3AN, United Kingdom

Executive Editor:
Tony Doré
Associate Editor:
Maëlis Arnould
Technical Editor:
Mohamed Gouiza

Reviewers:
Kim Welford
Carmen Gaina
Simon Williams

Submitted:
8 October 2024
Accepted:
10 January 2025
Published:
24 June 2025

Abstract Cretaceous to earliest Oligocene plate motions between Greenland and North America can only be directly modelled at high resolution from a short duration (61-42 Ma) sequence of magnetic isochrons in the Labrador Sea. Understanding those motions at other times is hampered by interpretational conflicts and the low or variable resolutions of geoscientific observations from west and north of Greenland. To better contextualize these observations, we build and manipulate models of North America-Eurasia and Eurasia-Greenland divergence and combine them to derive 13 new rotations that depict post-84 Ma North American-Greenland motions at unprecedented high temporal resolution. The rotations show that magnetic anomalies landwards of isochron C26 in the Labrador Sea cannot be related to magmatic crustal accretion at a focussed mid-ocean ridge. They also show how the North American-Eurasian plate boundary propagated northwards, leading to continental breakup in the Labrador Sea by ∼90 Ma and Baffin Bay by ∼68-65 Ma, perhaps in response to an increased supply of melt from the Iceland plume. We also show how field evidence for the Eurekan orogeny having occurred in distinct phases can be directly relatable to changes in Greenland-North American plate motion parameters over the 63-33 Ma period.

1 Introduction

Oceanic crust can deliver easily interpretable and high-precision constraints for studies of plate motion (cf. *Cox and Hart*, 1991). These constraints can however become difficult to identify unequivocally in geophysical data close to extended continental margins or where thin oceanic crust is the product of weak melt supply. Both of these sources of difficulty affect spreading-based studies of the relative motions of plates bearing Greenland and North America, which are recorded in the relatively narrow Labrador Sea and its even narrower neighbour Baffin Bay (Figure 1 and 2) (*Roest and Srivastava*, 1989; *Srivastava and Roest*, 1999; *Oakey*, 2005; *Oakey and Chalmers*, 2012; *Tappe et al.*, 2007; *Peace et al.*, 2016; *Larsen et al.*, 2009). The resulting uncertainties hinder attempts to generate a reliable plate kinematic-based interpretation context for the further northern reaches of the Greenland-North America plate boundary, a complex, remote, and in some aspects controversial Paleogene strike-slip and collision zone in northern Greenland and the Canadian Arctic archipelago known as the Eurekan Orogen.

In this work, we take a previously unused approach to modelling Greenland-North America relative plate motions. Estimates of finite rotation parameters in the wider plate circuit are optimized by maximizing the use of constraints from fracture zone locations. This enables us to calculate a plate motion model with higher resolution than those achieved in all previous studies, but without the need to employ disputed interpretations of seafloor markers from the Labrador Sea and Baffin Bay or field observations of convergent strain from north of Greenland. We use the model as a reliable independent context within which to refine and advance existing and new tectonic interpretations in those controversial settings.

1.1 Greenland/North America Motions: Previous Work and Observations

From the margins of the Labrador Sea and Baffin Bay, late Triassic or early Jurassic alkaline intrusions and earliest Cretaceous dykes have been understood as signs of slight continental extension (*Dickie et al.*, 2011; *Srivastava*, 1985), possibly leading to the formation of a mid-Cretaceous asymmetric rift (*Peace et al.*,

*✉ Graeme.Eagles@awi.de

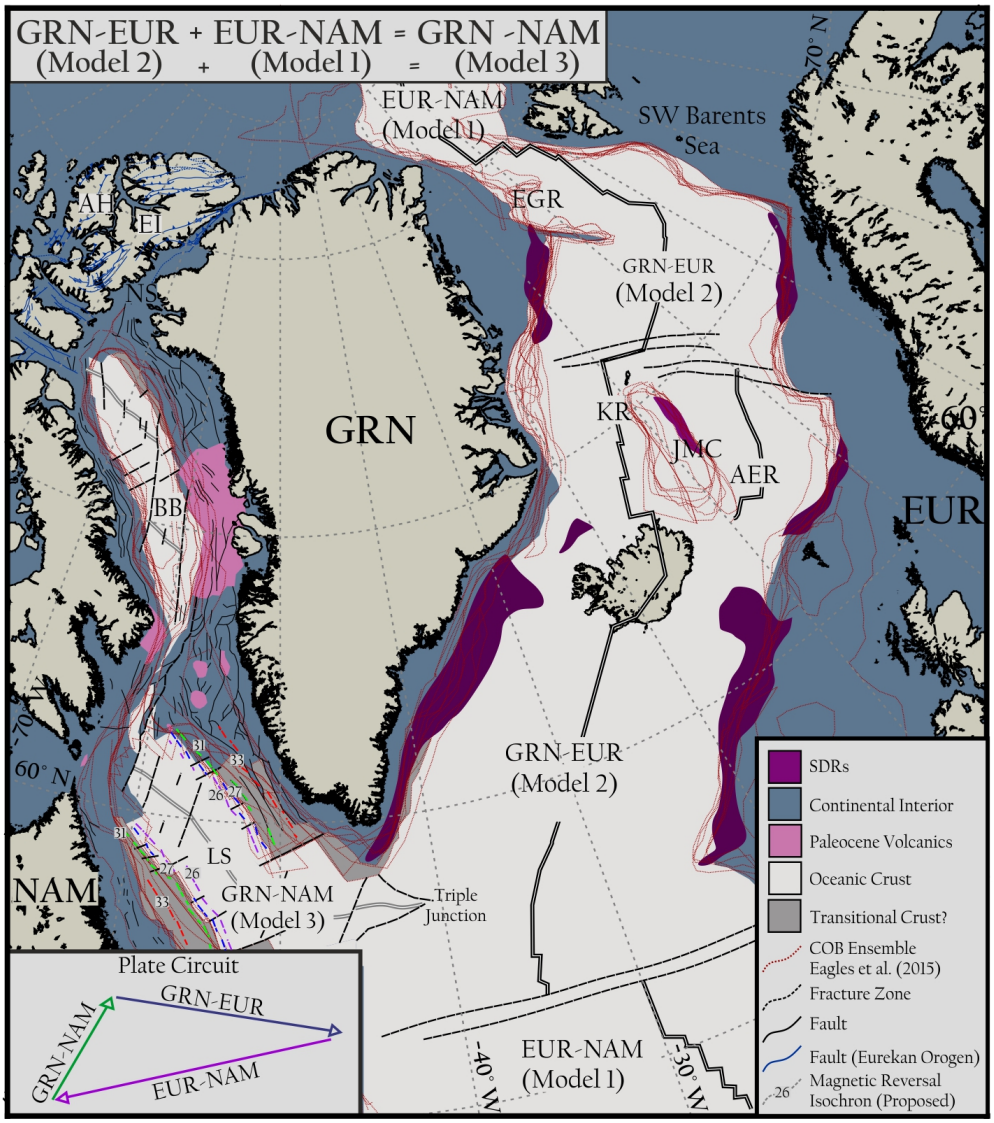

Figure 1 – Study region, some existing geological and tectonic interpretations, place names, and summary of the plate kinematic modelling approach using three models for divergence of the Greenland and Eurasian (GRN-EUR), Eurasian and North American (EUR-NAM) and Greenland and North American (GRN-NAM) plate pairs. AH: Axel Heiberg Island; BB: Baffin Bay; DS: Davis Strait; EGR: East Greenland Ridge; EI: Ellesmere Island; JMC: Jan Mayen Microcontinent; KR: Kolbeinsey Ridge; LS: Labrador Sea. SDRs (seaward dipping reflector sequences) mapped from *Larsen and Saunders* (1998); Transitional crust, volcanics, faults, and fracture zones west and north of Greenland from *Oakey and Stephenson* (2008) and *Piepjohn et al.* (2016); Atlantic and Ægir ridge crests and fracture zones interpreted from satellite-derived gravity anomaly data (*Sandwell et al.*, 2014). Coloured symbols in Labrador Sea: magnetic isochron picks collated by *Seton et al.* (2014).

2016). Sedimentation in fault-bounded basins started in the Early Cretaceous, and gave way to breakup and regional thermal subsidence at a poorly constrained time later in the Cretaceous (*Dickie et al.*, 2011). Studies of plate motion after this time rely heavily on magnetic anomaly identifications from the Labrador Sea (*Roest and Srivastava*, 1989; *Srivastava and Roest*, 1999; *Oakey*, 2005; *Oakey and Chalmers*, 2012; *Srivastava*, 1985) (Figure 1). From these, there is near consensus (*Chalmers*, 1991; *Chalmers and Laursen*, 1995) that steady-state seafloor spreading was underway in Paleocene times, by the normal polarity phase of either chron C27 or C26 (62.52 or 59.24 Ma; *Srivastava and Roest*, 1999; *Keen et al.*, 2018; *Gradstein et al.*, 2012) (Figures 1 and 2). In that period, synchronous regional large-volume magmatism driven by lithospheric and sub-lithospheric processes produced lava flow piles, sills and lower crustal bodies of the North Atlantic Igneous Province, its products interpretable in seismic reflection data and returned in drill cores from both west and east of Greenland (Figure 2 *Geissler et al.*, 2017; *Hopper et al.*, 2004; *Gaina et al.*, 2017; *Larsen and Saunders*, 1998). This magmatic event was swiftly followed at ∼56 Ma by a fundamental change in plate divergence azimuth in the Labrador Sea, which has been related to the onset of seafloor spreading off eastern Greenland (*Oakey and Chalmers*, 2012). After this, the youngest consistently identifiable magnetic reversal isochron in the Labrador Sea is C20 (43.43-42.30 Ma), but ∼30 km of younger rugged oceanic basement lies between it and the extinct mid-ocean ridge. North Atlantic magnetic isochrons near the South Greenland Triple Junction suggest this seafloor accreted until around 33 Ma (*Kristoffersen and Talwani*, 1977).

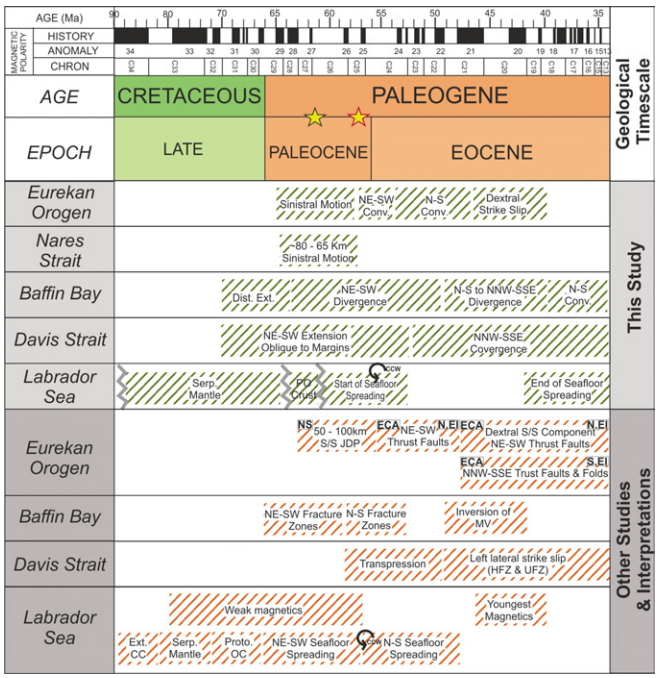

Figure 2 – Summary of new and previous interpetations (see *Abdelmalak et al.*, 2019; *Chalmers*, 1991; *Chalmers and Laursen*, 1995; *Delescluse et al.*, 2015; *Harrison et al.*, 2006; *Harrison and Jackson*, 2008; *Harrison et al.*, 2011; *Harrison and Jackson*, 2014; *Keen et al.*, 2018; *Knutz et al.*, 2012; *Oakey*, 2005; *Oakey and Chalmers*, 2012; *Roest and Srivastava*, 1991; *Srivastava and Keen*, 1995; *Tessensohn and Piepjohn*, 2000; *Torsvik et al.*, 2008) of tectonic evolution west and north of Greenland since late Cretaceous times. Dist. Ext: distributed extension; ECA: eastern Canadian Arctic; Ext. CC: extended continental crust; HFZ: Hudson fracture zone; MV: Melville Graben; N.EI: northern Ellesmere Island; NS: Nares Strait; Proto. OC/PO crust: proto-oceanic crust; S.EI: southern Ellesmere Island; S/S JDP: strike-slip Judge Daly Peninsula; UFZ: Ungava fracture zone.

The crust marginwards of C26-C27 in the Labrador Sea, and thus its earliest Paleocene and earlier history is less well understood. Weak magnetic anomaly lineations have been suggested to represent polarity reversal isochrons raised over thin igneous crust formed at distributed sites within broad continent-ocean transition zones (COTZs) (*Gillard et al.*, 2016; *Stanton et al.*, 2016; *Keen et al.*, 2018). Alternative interpretations of these anomalies exist, for example that they may relate to serpentinization of exposed mantle rocks in slow spreading settings (*Sibuet et al.*, 2007). It remains open to question whether such settings might produce dateable linear magnetic reversal isochrons like those over standard (~7 km-thick) oceanic crust and, thus, whether picks of reversal isochrons as old as C33 (79.9-74.31 Ma) (*Roest and Srivastava*, 1989; *Srivastava and Tapscott*, 1986) are reliable (Figure 2).

To the north of the Labrador Sea, Davis Strait hosts prominent N-S trending fault zones (Figure 1) that are widely understood to have facilitated the development of Paleocene-Eocene aged sheared continental margin segments (*Chalmers and Pulvertaft*, 2001; *Funck et al.*, 2007, 2012; *Hosseinpour et al.*, 2013; *Suckro et al.*, 2012). Between these margins, the crustal affinity beneath the floor of Davis Strait is uncertain (*Tucholke and Virginia*, 1985; *Chalmers and Pulvertaft*, 2001; *Srivastava*, 1983; *Larsen and Williamson*, 2020; *Longley et al.*, 2024). Further north still, wide-angle seismic profiles (*Funck et al.*, 2012; *Suckro et al.*, 2012; *Reid and Jackson*, 1997; *Altenbernd et al.*, 2014) and a well-defined extinct median valley in gravity anomalies (*MacLeod et al.*, 2017) show that central Baffin Bay is floored by oceanic crust and/or exhumed mantle rocks. Baffin Bay lacks strong magnetic lineations (*Reid and Jackson*, 1997; *Keen and Barrett*, 1972; *Keen et al.*, 1974). Consequently, its plate kinematic history is understood by extrapolation from the Labrador Sea, suggesting it was the site of an active mid-ocean ridge until ~33 Ma.

North of Baffin Bay, evidence for Paleogene continental collision is widespread in the Canadian Arctic islands, particularly Ellesmere Island (*Oakey and Chalmers*, 2012; *Harrison et al.*, 2011; *Gion et al.*, 2017) (Figure 1). Understanding of the collision belt, known as the Eurekan Orogen, is complicated by strong overprinting relationships affecting the fold and fault structures it comprises. Many of its faults appear to be reactivated Paleozoic thrusts. Many show marked strike-slip components (*Tessensohn and Piepjohn*, 2000; *Piepjohn et al.*, 2016). Field-based estimates of Eurekan orogenic shortening are consequently subject to considerable numerical and interpretational uncertainties, but otherwise broadly consistent with the history of Greenland-North America motion as it is understood from plate kinematic models of the Labrador Sea (*Oakey and Chalmers*, 2012; *Srivastava*, 1985; *Srivastava and Tapscott*, 1986; *Gion et al.*, 2017; *Tessensohn and Piepjohn*, 2000; *Saalmann et al.*, 2005). Most of these models however imply the occurrence of ~300 km or more of sinistral strike motion parallel to the northern Greenland margin (*Roest and Srivastava*, 1989), which is irreconcilable with field evidence for just 50-100 km from Ellesmere Island (*Gion et al.*, 2017; *Saalmann et al.*, 2005; *Harrison and Jackson*, 2014).

1.2 Aims and Objectives

Software advances have relatively recently enabled plate motions to be modelled using deformation estimates derived from geophysical and outcrop-based studies of extensional and convergent plate boundary zones west and north of Greenland (*Hosseinpour et al.*, 2013; *Gion et al.*, 2017; *Welford et al.*, 2018). The accuracies of the results of these approaches are bound up with large uncertainties in their inputs and also depend on a priori assumptions about the rigid plate motion azimuths that deformation responds to (*Eagles et al.*, 2015). Here, we take a complementary approach that derives relative Greenland-North American plate motions independently of any observations or a priori assumptions from studies of the Labrador Sea, Davis Strait, Baffin Bay or Canadian Arctic. We apply a proven inversion technique (*Nankivell*, 1997; *Livermore et al.*, 2005; *Eagles*, 2004) to published picks of seafloor isochrons (*Klitgord and Schouten*, 1986; *Gaina et al.*, 2002, 2009) and picks of tectonic flowline features in satellite altimeter data (*Sandwell et al.*, 2014) to generate

two sets of finite rotations that portray relative motions of 1) the Eurasian and North American (EUR-NAM) plates and 2) the Greenland and Eurasian (GRN-EUR) plates. The rotation sets feature high (1-5 Myr) temporal resolution and are supported by quantified uncertainty estimates. Under the assumption that the interiors of the three plates remained rigid (e.g., *Cox and Hart*, 1991), we sum the two sets of rotations to derive a third, which describes relative motions of the Greenland and North America (GRN-NAM) plates. Because the input rotations are derived only from interpretations of magnetic anomaly isochrons and fracture zone traces east and northeast of North America and Greenland (Figure 1, and Supplementary Figures S1 and S2), the summed rotations are insensitive to the imprecise or conflicting constraints that come from interpretations of geological and geophysical observations in the complex narrow basins between them.

Our circuit-derived plate motion history for Greenland with respect to North America allows us to provide new independent estimates of the timing and azimuth of plate divergence in the Labrador Sea during its history of lithospheric necking, COTZ formation and, ultimately, accretion of oceanic crust. Using the estimates, we also speculate on the roles of pre-existing extensional structures in oblique seafloor spreading. Our results further enable us to better understand the opening of narrow basins floored by transitional and/or oceanic crust in Davis Strait and Baffin Bay, and their alteration by later plate convergence, contextualizing independent observations of compressional structures in both. Further north still, we compare the detailed plate motion history described by our model to strain estimates derived from field-based studies of the Eurekan orogen.

2 Data

The North Atlantic is one of the most densely surveyed deep ocean regions for magnetic anomaly data anywhere on Earth. Many hundreds of long magnetic profiles are available, revealing in close detail the presence of multiple coherent continuous high amplitude anomalies that uphold a long-lived consensus on the identities and locations of geomagnetic reversal isochrons (e.g., *Macnab et al.*, 1995; *Merkouriev and DeMets*, 2008). In addition to these, satellite altimetry data provide the region south of 80°N with continuous gridded gravity anomaly coverage at a full wavelength resolution of around 12 km (*Sandwell et al.*, 2014). Ship- and aircraft-based gravity data further north are available also as a grid, albeit with a more variable resolution that depends on local details of vehicle track spacing and orientations (*Gaina et al.*, 2011). Using these resources, we gathered data sets suitable for modelling relative motions of the Greenland-Eurasia (GRN-EUR) and Eurasia-North America (EUR-NAM) plate pairs.

Table 1 – Chron labels used here and by *Gradstein et al.* (2012), with ages rounded to nearest 10 ka. Edge refers to the young (y) or old (o) end of the interval or edge of the corresponding signal.

Label in this paper	*Gradstein et al.* (2012) label(edge)	*Gradstein et al.* (2012) age
C2	C2n(y)	1.78
C2A1	C2An.1n(y)	2.58
C2A3	C2An.3n(o)	3.60
C3n1	C3n.1n(y)	4.19
C3n4	C3n.4n(o)	5.24
C3A	C3An.2n(o)	6.73
C4n1	C4n.1n(y)	7.53
C4n2	C4n.2n(o)	8.11
C4A	C4An(o)	9.11
C5n1	C5n.1n(y)	9.79
C5n2	C5n.2n(o)	11.06
C5C	C5Cn.1n(y)	15.97
C5D	C5Dn(y)	17.24
C5E	C5En(y)	18.06
C6	C6n(o)	19.72
C13	C13n(y)	33.16
C18	C18n.2n(o)	40.15
C20	C20n(o)	43.43
C21	C21n(o)	47.35
C22	C22n(o)	49.34
C24	C24n.3n(o)	53.98
C25	C25n(y)	57.10
C26	C26n(o)	59.24
C27	C27n(o)	62.52
C28	C28n(o)	64.67
C29	C29n(o)	65.69
C31	C31n(y)	68.37
C33	C33n(o)	79.90
C34	C34n(y)	83.64

2.1 Geomagnetic Reversal Anomaly Isochrons

The first data set is of seafloor isochron locations (Supplementary Figure S1). We sourced picks of magnetic polarity reversal isochrons C6 (19.72 Ma) and younger (*Merkouriev and DeMets*, 2008) and of older isochrons reaching as far back as C34 (83.64 Ma) (*Gaina et al.*, 2002; *Macnab et al.*, 1995) from an online repository (Seton et al., 2014), and dated them according to a recent reversal timescale (Table 1 *Gradstein et al.*, 2012). For the EUR-NAM model, we added around 200 new picks for chrons C26, C27, C28, and C29, using freely available ship track data (*NOAA National Geophysical Data Center*, 2023). The GRN-EUR model, which describes seafloor spreading with a later onset, is constrained by picks of a subset of isochrons in the sequence C24-C6 (53.98-19.72 Ma) (*Gaina et al.*, 2002). From these basins, we use picks of C6 and the anomalies ridgewards of them, which post-date independent motion of the Greenland Plate, as input for our EUR-NAM model. In total, the isochron pick data sets amount to 9516 data, of which 1626 are used for the GRN-EUR model and 7890 for the EUR-NAM model.

2.2 Accretionary Flowline Traces

Along-axis variability in tectonic and magmatic processes at mid-ocean ridges leaves observable traces in the structure of the oceanic crust they create. If the sources of this variability do not migrate along the ridge crest, then the traces they produce are reliable records of the azimuth of relative plate motion responsible for the

ridge's action. Numerous such features, which we refer to here as accretionary flowline traces, can be observed in the North Atlantic and Arctic oceans, and form the second of our input data sets.

We picked accretionary flowline traces south of 80°N from anomalies in satellite altimetry-derived free air gravity estimates (*Sandwell et al.*, 2014), and further north from a gridded compilation of near-surface gravity anomaly measurements (*Gaina et al.*, 2011) (Supplementary Figure S2A and S2B). We picked at 5 km intervals in the altimetry-derived data, and at 10 km intervals in the less uniform Arctic data set (Supplementary Figure S2C). We initially selected candidate features for picking based on visual comparison to synthetic flowline segments calculated for previous rotation models of the region (*Gaina et al.*, 2002, 2009). The most reliable accretionary flowline traces are those that can be attributed to the deep continuous narrow basement valleys that characterize transform faults and the fracture zones that form where they intersect mid-ocean ridge crests. These include the Charlie Gibbs and Bight fracture zones (Supplementary Figure S2A). Further north we picked along the footwalls of the Paleocene to Eocene aged Greenland and Senja Fracture Zones (Supplementary Figure S2) rather than the adjacent troughs, which appear to have widened during Oligocene and later cross-axial extension (*Døssing and Funck*, 2012). We also picked parts of the Eastern Jan Mayen Fracture Zone (Supplementary Figure S2) that lie marginward of its C21-aged paleo ridge-transfrom intersection on the Eurasian plate. We omitted the younger parts of this fracture zone because they can be suspected to record relative motion of a small independently moving plate bearing the Jan Mayen microcontinent (Figure 1 *Gaina et al.*, 2009). Non-transform related accretionary flowline traces tend to appear as shorter and often subtler troughs or ridge features. As well as by comparing them to synthetic flowline segments, we carefully validated candidates for such traces by checking for magnetic isochron offsets across them. Amongst them, we picked two linear step-like features near the edges of the Greenland-Iceland and Iceland-Faroe ridges, and a small number of troughs and trough-step features in the Arctic Ocean (Supplementary Figures S2B and S2C). In total, we picked 754 accretionary flowline crossings for the GRN-EUR model, and 1743 for the EUR-NAM model. The total, 2497 crossings, is two orders of magnitude greater than that used by *Gaina et al.* (2002, 2009) for their models of the same plate pairs.

2.3 Necking Zone Data

The sequence of magnetic reversal anomalies formed in GRN-EUR divergence begins with C24 (∼54 Ma). Landwards of C24 lie COTZs that formed before 54 Ma in a complex interplay of magmatic and mechanical processes. The diverse internal architectures of COTZs have long proved difficult or controversial to interpret in terms of the detailed history of plate divergence. Crustal necking zones, in contrast, are obligate features of the landward edges of COTZs that are relatively easy to understand as products of focussed crustal thinning. This focussing occurs early on during continental breakup, typically reducing crustal thicknesses of ∼35 km or more to ∼10 km or less (e.g., *Pérez-Gussinyé and Reston*, 2001; *Chenin et al.*, 2017, 2018). Necking tends to produce large basement topographic signals, which raise prominent gravity anomalies. These anomalies show some complexity where the necking zone coincides with prograded sediment bodies and extensive igneous additions to the COTZ (*Watts and Fairhead*, 1999). Elsewhere they have been shown to be indistinguishable from the locations of restored (pre-extensional) seaward edges of continental crust at the level of coarse (∼100 km) resolution achievable by COTZ restoration techniques (*Eagles et al.*, 2015; *Barnett-Moore et al.*, 2016). COTZ restorations require assumptions to be subjectively made about various boundary and developmental conditions. Crucially, one of these assumptions, about the azimuth of plate motion during COTZ development, requires choosing a set of existing Euler rotation parameters for the earliest phase of plate divergence. As this choice contributes to the shape and position of the resulting restored plate edge, it goes on to influence the rotation parameters that describe the pre-kinematic reconstruction. Directly picking the necking zone edge, in contrast, requires no such knowledge, leaving our inversion procedure free of a priori influences on the constraints used for its earliest stage.

The small set of twelve necking zone edge picks in our model (Figure 3 and Supplementary Figure S1) are taken from prominent edges in free-air gravity over short segments of the continental shelves in the Iceland and Irminger basins, landward of their identified seaward dipping reflectors (*Larsen and Saunders*, 1998). The picks are labelled as "GEN". In picking GEN, we assume that the necking zones formed during continental breakup, and the necking itself to have been a process that completed rapidly enough for us to treat its products, the short shelf edge segments, as isochrons. Consistent with the first of these assumptions, Figure 3 shows that the GEN picks lie towards or beyond the landwards limits of the ensembles of around fifteen published COB estimates for each of the basin margins (*Eagles et al.*, 2015). Figure 3 also confirms, as cited above, that the spacing of the GEN picks is indistinguishable from that of the quantitatively restored pre-rift plate edge, within its estimated 100 km uncertainty (*Barnett-Moore et al.*, 2016).

3 Methods

3.1 Inverse Derivation of EUR-NAM and GRN-EUR Rotations

We use a well-established joint inversion technique for magnetic isochron and fracture zone location data (*Nankivell*, 1997; *Livermore et al.*, 2005; *Eagles*, 2004) to determine twenty-nine sets of finite rotation parameters for EUR-NAM (for times in the period 83.64-0 Ma) and seven (for the period 57.10-19.72 Ma) for GRN-EUR relative motions (Tables 2 and 3; Figures 4-7). Two

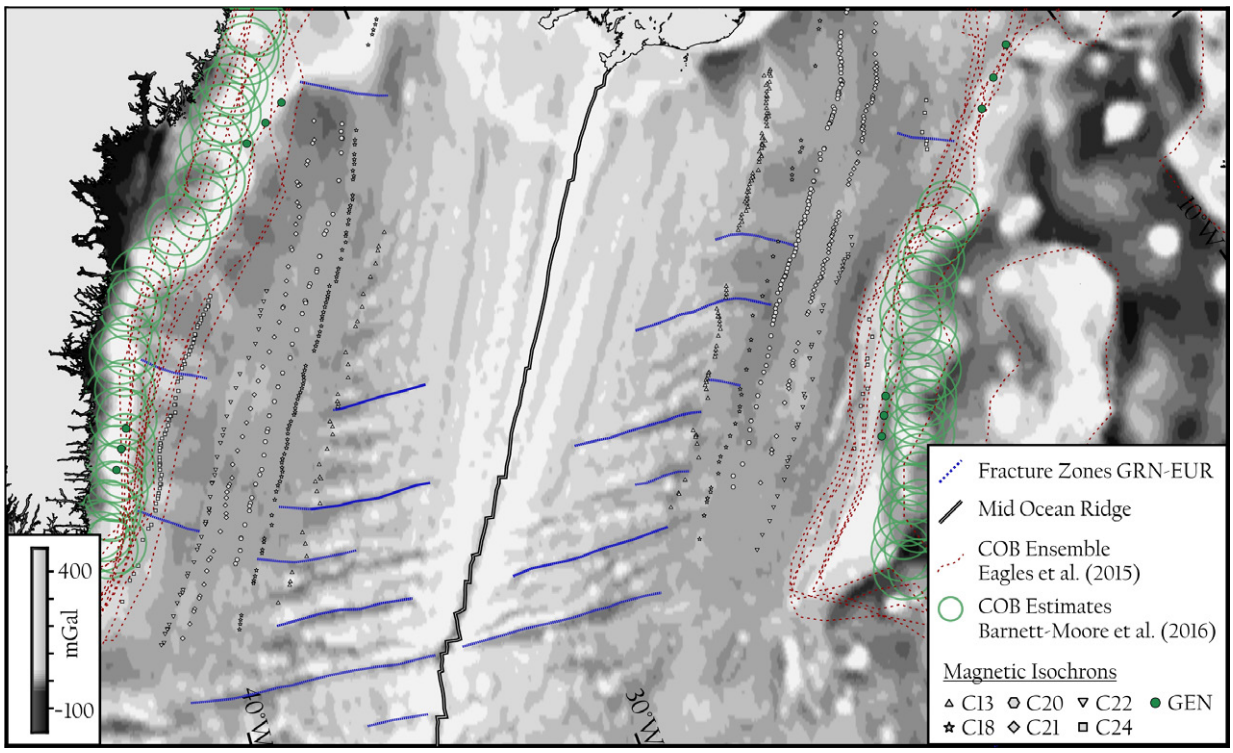

Figure 3 – GEN picks compared to restored COB estimates from *Barnett-Moore et al.* (2016) (yellow disks with 100 km diameters illustrating estimated uncertainty of the restoration) and ensemble of 15 North Atlantic COB estimates (*Eagles et al.*, 2015). Other features as in previous figures.

sets of misfits are generated and the root mean squares of their magnitudes are progressively minimized using a ridge regression procedure based on the Lanczos process (see *Paige and Saunders*, 1982) until a model with satisfactory misfit (i.e. with misfit population standard deviations within the 0-15 km range expected for navigational, observational, and geological uncertainty in features along divergent plate boundaries) is achieved. One set of misfits is calculated between picks of accretionary flowline features observed in gravity data and synthetic ridge-crest flowlines constructed as chains of small-circle segments drawn about consecutive stage rotations calculated from the current set of finite rotations for the two diverging plates. The second set is calculated between picks of seafloor isochrons after rotating them about the current set of finite rotations, and great circle segments defined by least-squares fitting to chosen groups of target picks. Target groups in the EUR-NAM model were exclusively composed of conjugates to the rotating picks. Conjugate targets also dominate in the GRN-EUR model, but here we also allowed for a small number of non-conjugate targets to be defined and fitted using appropriate stage rotations in order to enable the use of C21 and older magnetic isochron data from the Eurasian flank of the Ægir Ridge.

Eagles (2019), in a supplement, compares our joint inversion technique in detail to the widely used alternative technique of *Hellinger* (1981), which forms the basis of the most influential previous inverse studies of GRN-EUR and EUR-NAM plate divergence (*Gaina et al.*, 2002, 2009). The comparison describes how our technique optimizes the use of accretionary flowline traces; it considers their entire lengths by regarding them in a kinematically correct way as the traces of stationary points, such as ridge-transform offsets, on evolving mid-ocean ridge crests. The Hellinger approach, in contrast, employs only those parts of such zones that offset magnetic isochrons, and also treats pairs of them as the conjugate walls of paleo-transform faults. Such a treatment is bogus, owing to the finite offset of the transform fault at whose ends the two fracture zones formed (*Shaw and Cande*, 1990; *Nankivell*, 1997). These differences are particularly consequential in the North Atlantic models presented here, where the majority of available isochron offsets are quite short. This condition restricted *Gaina et al.* (2002, 2009) to the use of just a handful of flowline crossings. Our technique's optimization of fracture zone constraints tends to produce models that imply smoother plate motion histories than alternative approaches (Supplementary Figure S3). Such histories are more consistent with the long (tens of Myr) expected evolutionary timescales of plate driving forces and their balance than the jerkier histories sometimes implied by the results of Hellinger-type inversions.

3.2 Derivation of GRN-NAM Rotations by Plate Circuit Closure

Assuming plates are internally rigid, then the sum of the rotations describing plate motions across any set of plate boundaries that begins and ends on the same plate (a so-called plate circuit) will be zero. In previous work on the region, *Gaina et al.* (2002) iteratively approached a set of rotations that satisfy this condition within error, by simultaneously modelling relative motions on all three arms of the GRN-NAM-EUR plate system

Table 2 – Finite rotation parameters and covariances for model motion of Eurasian plate with respect to North American plate.

LAT, λ	LON, Φ	ANG, θ	CHRON	λ,λ	λ,Φ	λ,θ	Φ,Φ	Φ,θ	θ,θ
-56.41	-47.94	0.38	C2	8.19629E-01	1.73821E-01	-2.88754E-03	1.52586E-01	-4.96160E-04	1.19900E-05
-61.47	-46.34	0.57	C2A1	1.77792E-01	1.30749E-02	-1.27810E-03	8.79770E-02	1.74240E-05	1.09989E-05
-62.81	-44.83	0.79	C2A3	1.97865E-01	5.01071E-02	-1.86145E-03	8.37869E-02	-3.39395E-04	2.00951E-05
-62.74	-44.89	0.92	C3n1	2.10426E-01	4.42083E-02	-2.36541E-03	8.64916E-02	-2.37207E-04	3.05541E-05
-63.63	-45.74	1.14	C3n4	1.30472E-01	2.69379E-02	-1.88667E-03	5.46824E-02	-2.29574E-04	3.07245E-05
-64.67	-46.35	1.40	C3A	1.13398E-01	2.10734E-02	-2.12033E-03	4.32384E-02	-2.71864E-04	4.39009E-05
-65.54	-45.97	1.65	C4n1	5.14109E-02	8.77689E-03	-1.23642E-03	2.80333E-02	-6.81726E-05	3.42819E-05
-65.86	-46.04	1.83	C4n2	3.85211E-02	4.23466E-03	-1.09179E-03	2.46749E-02	-4.33075E-06	3.53033E-05
-66.34	-47.61	2.11	C4A	4.91010E-02	7.50663E-03	-1.59143E-03	2.68320E-02	-6.98193E-05	5.74218E-05
-67.15	-48.48	2.30	C5n1	1.14533E-02	-1.17561E-03	-4.67113E-04	1.27543E-02	8.55313E-05	2.33777E-05
-67.93	-48.06	2.65	C5n2	4.29953E-03	-4.49893E-04	-2.23953E-04	3.02427E-03	2.82796E-05	1.35059E-05
-68.50	-47.75	4.08	C5C	1.31857E-02	4.48864E-03	-8.42863E-04	6.12329E-03	-2.41095E-04	6.11675E-05
-68.63	-47.44	4.48	C5D	1.37912E-02	6.97548E-03	-9.54319E-04	1.18950E-02	-3.89015E-04	7.50964E-05
-68.75	-47.37	4.70	C5E	1.27750E-02	5.08044E-03	-9.27302E-04	9.57226E-03	-2.15720E-04	7.70500E-05
-68.75	-46.30	5.08	C6	3.94533E-03	1.24260E-03	-3.21235E-04	1.99195E-03	-8.23316E-05	2.93768E-05
-68.82	-45.10	7.74	C13	4.87305E-03	7.01826E-04	-5.50248E-04	1.24159E-03	-1.20070E-04	9.31416E-05
-67.81	-43.05	9.21	C18	1.65189E-03	5.03326E-06	-2.78315E-04	1.70710E-03	-6.07609E-05	7.16238E-05
-66.24	-41.05	9.89	C20	1.76160E-03	-7.30476E-05	-2.36039E-04	1.59726E-03	-5.08111E-05	5.08880E-05
-65.35	-40.25	10.96	C21	1.79645E-03	8.30167E-05	-2.74787E-04	1.98073E-03	-8.00451E-05	6.44079E-05
-64.77	-40.03	11.54	C22	1.46776E-03	-3.87309E-06	-2.39225E-04	1.49480E-03	-6.60110E-05	6.16655E-05
-62.87	-38.54	12.77	C24	1.80986E-03	2.20624E-04	-2.76284E-04	1.01563E-03	-1.35602E-04	7.52060E-05
-60.66	-37.32	13.64	C25	5.98910E-02	6.53395E-03	-5.69103E-03	2.17656E-03	-7.55609E-04	5.70212E-04
-56.86	-35.47	13.92	C26	8.83958E-02	3.61672E-03	-6.63140E-03	2.58931E-03	-4.45485E-04	5.33725E-04
-54.11	-34.72	14.44	C27	1.31102E-01	7.84814E-03	-7.68010E-03	3.89799E-03	-6.48933E-04	4.93690E-04
-54.58	-33.85	15.00	C28	9.85053E-01	2.64364E-02	-4.88866E-02	5.42010E-03	-1.65918E-03	2.53337E-03
-55.05	-33.91	15.36	C29	1.03585E-01	2.96462E-03	-7.79472E-03	2.98025E-03	-5.82109E-04	6.63332E-04
-56.10	-33.14	15.98	C31	4.95773E-02	9.64911E-04	-3.84220E-03	8.50669E-04	-1.69846E-04	3.22927E-04
-60.38	-32.03	18.09	C33	2.54648E-02	-2.48419E-04	-2.88295E-03	6.35147E-04	-8.70760E-05	3.59000E-04
-60.98	-31.71	18.91	C34	2.45986E-02	-1.81660E-03	-2.59903E-03	1.73885E-03	-1.56201E-04	3.59875E-04

Table 3 – Finite rotation parameters and covariances for model motion of Greenland plate with respect to Eurasian plate.

LAT, λ	LON, Φ	ANG, θ	CHRON	λ,λ	λ,Φ	λ,θ	Φ,Φ	Φ,θ	θ,θ
68.49	133.93	5.06	C6	0.35824E-02	0.12497E-02	0.32547E-03	0.20551E-02	0.13553E-03	0.40707E-04
68.73	134.92	7.82	C13	0.17580E-01	-0.39312E-02	0.24456E-02	0.21511E-02	-0.49335E-03	0.38156E-03
61.01	132.94	8.39	C18	0.28618E-01	-0.67341E-02	0.30657E-02	0.35406E-02	-0.65604E-03	0.36037E-03
57.68	130.91	8.73	C20	0.19697E-01	-0.50334E-02	0.21517E-02	0.44010E-02	-0.41979E-03	0.26489E-03
53.17	129.57	9.31	C21	0.20571E-01	-0.39987E-02	0.20764E-02	0.34031E-02	-0.30750E-03	0.23356E-03
49.59	128.88	9.49	C22	0.19132E-01	-0.40381E-02	0.17312E-02	0.26817E-02	-0.31017E-03	0.18260E-03
52.22	123.15	11.48	C24	0.18189E-01	-0.52558E-02	0.26935E-02	0.26333E-02	-0.80089E-03	0.43923E-03
54.89	120.43	12.79	GEN	0.33289E+00	-0.11800E+00	0.41874E-01	0.44463E-01	-0.14953E-01	0.56491E-02

during the C24-C13 (∼54-33 Ma) period. Here, in contrast, we make explicit use of the same condition as an assumption, calculating C24 and younger-aged rotations for the GRN-NAM pair by summing those for the GRN-EUR and EUR-NAM plate pairs. Statistical confidence regions for the resultant rotations were calculated by numerically convolving rotations sampled from the interiors of the summed rotations' individual confidence ellipses.

We investigated pre-C24 plate divergence in the Labrador Sea in terms of EUR-NAM plate divergence, under the assumption that Greenland would have moved as part of a rigid Eurasian plate prior to the onset of EUR-GRN divergence. To do this, we calculated a set of EUR-NAM rotations for periods ending at the date of the GEN rotation, when rapid focussed EUR-GRN motion started, and summed each of them to the EUR-GRN rotation for GEN to generate full finite rotations to the end of EUR-GRN plate divergence. To enable this, we assume that GEN coincides in time with C25, the immediate predecessor of C24, the oldest consistently observed reversal isochron between the Greenland and Eurasian conjugate margins. We will examine the validity of this assumption later.

4 Results

4.1 Eurasia – North America Plate Divergence

The solution for the EUR-NAM plate pair is listed in Table 2, and shown in Figure 4 as sets of visual fits of isochron picks and synthetic ridge-crest flowlines rotated to target great circle segments and fracture zone traces. The technique reduces misfits to means and standard deviations of -0.07 km and 4.99 km for magnetic isochron data and 0.00 km and 3.67 km for accretionary flowline data.

Figure 5 shows the locations of the 29 new finite rotation poles and their associated 95% confidence ellipses, describing the relative divergence of Eurasia and North America since the Late Cretaceous (C34; ∼84 Ma). The progression of the poles is on the whole similar

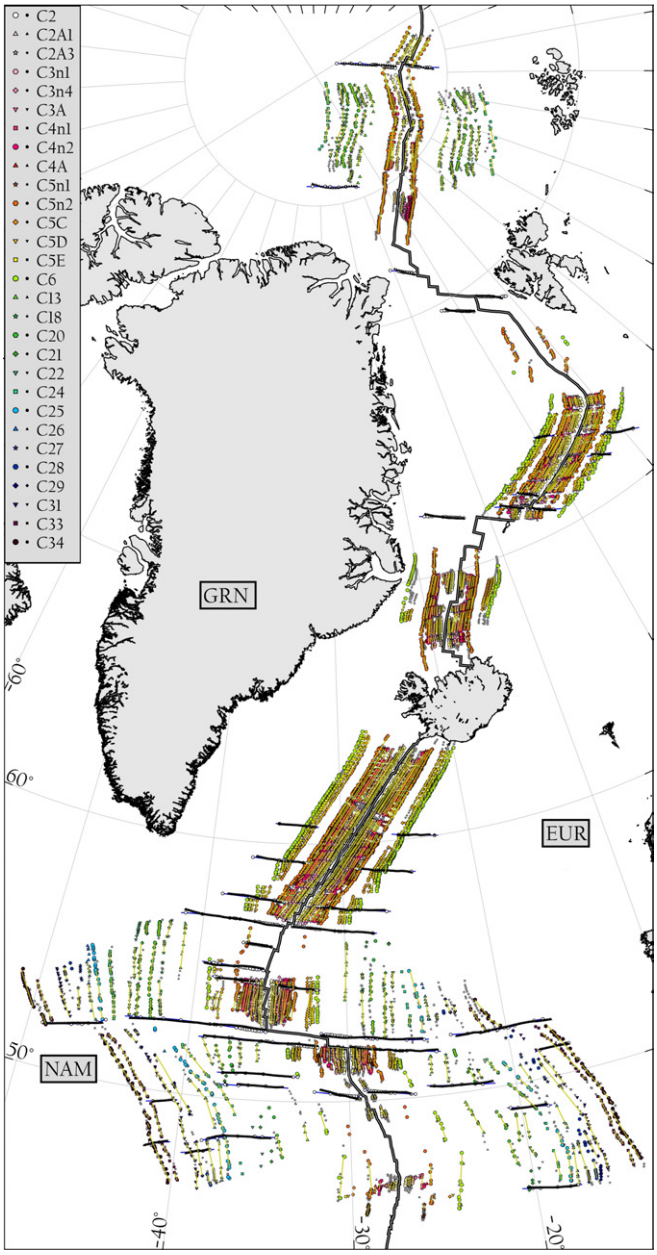

Figure 4 – Visual representation of fits in the EUR-NAM model. Coloured symbols: fixed isochron picks as in Supplementary Figure S1. Grey symbols: isochron picks after rotation in model. Yellow lines: great circle fitting targets based on isochron pick groupings. Small black triangles: accretionary flowline picks from Supplementary Figure S2. Blue lines: synthetic flowline segments designed to fit them. Double lines: modern plate boundaries from *Bird* (2003). A larger scale version of this figure is included as Supplementary Figure S4 to enable closer inspection.

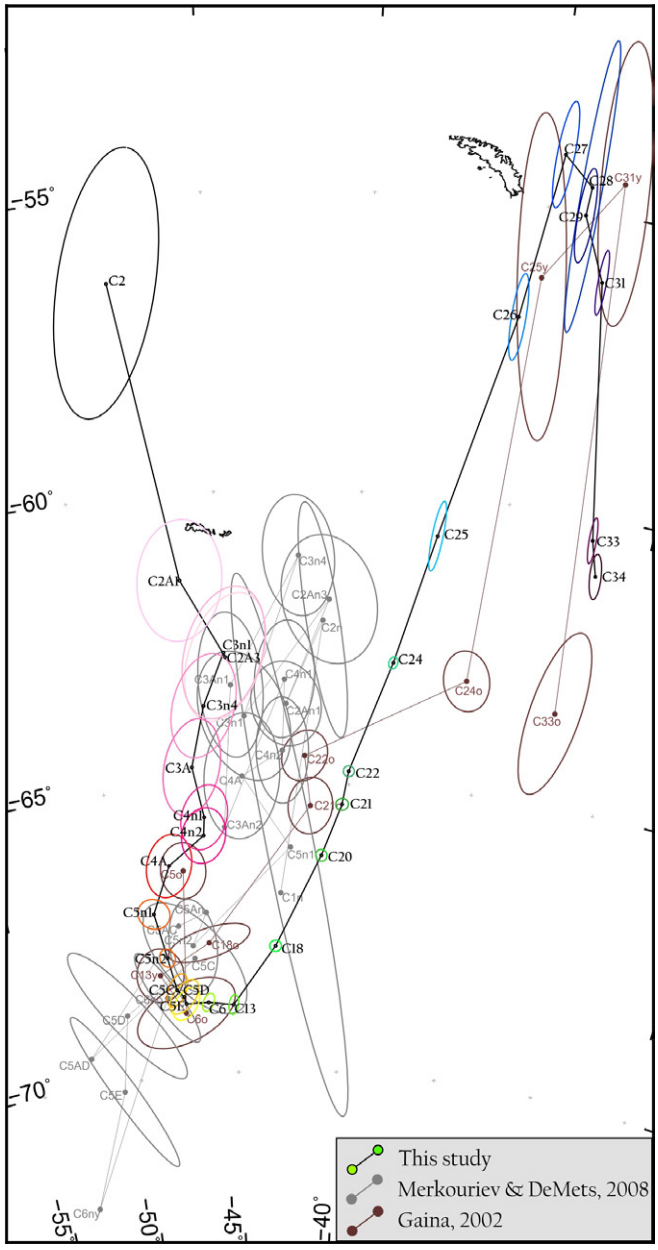

Figure 5 – Locations of the new EUR-NAM rotation poles and their 95% confidence ellipses, derived analytically from the covariances in Table 2. The colours of the ellipses correspond to those used for the picks in Figure 4. Pole sets and graphically reproduced confidence regions from two previous studies are shown to aid the comparison described in the text.

to, but considerably smoother than, the progressions in the earlier studies of *Merkouriev and DeMets* (2008) and *Gaina et al.* (2002). As noted above, this smoothness might be expected of major plate motions and, as experience has shown, is a reflection of the much better use of accretionary flowline data that our method is able to make. The progression implies three distinct phases of relative plate motion, punctuated by inflections at C13 (~33 Ma, Eocene-Oligocene boundary) and C27 (~63 Ma, early Paleogene).

The elliptical 95% confidence regions are somewhat smaller than those of previous studies. This too is a direct consequence of the much greater amenability of flowline constraints to our method. In more detail, the ellipses for the younger rotations tend to be larger than those for the older rotations, an expected consequence of their tighter Euler angles. As well as this, the ellipses for the pre-C24 poles are larger than for post-C24 ones because of the absence of pre-C24 constraints from north of the Greenland Triple Junction. Few of the new poles plot within the 95% confidence regions around previous ones. The previously published poles that come closest to our new counterparts are those that used Labrador Sea data for triple junction closure in the period C24-C13 (*Gaina et al.*, 2002). From this, we conclude that the

capability for flowline fitting is of comparable benefit to our two plate models as is the addition of data from two further arms of a plate circuit to a Hellinger-type model, upgrading it from a two- to a three-plate model.

4.2 Greenland – Eurasia Plate Divergence

The GRN-EUR solution is shown in Figure 6 and Table 3. Including outliers, the means of isochron and accretionary flowline misfits are -0.43 km and 0.00 km, and their standard deviations are 8.29 km and 2.77 km. Fits to the flowlines do not show any large outliers. Outliers among the rotated magnetic isochron picks occur in small groups, often near the tips of paleo-ridge segments scattered throughout the data set. This distribution leaves little reason to suspect our data selection ought to recognize the motion of a third plate, bearing the Jan Mayen microcontinent, as *Gaina et al.*'s (2009) separate treatment of the two pairs of basins north and south of Iceland was designed to demonstrate. The remnants of the Jan Mayen plate are thus likely to be confined to the Norway Basin between the Ægir and ancestral Kobeinsey ridges.

Figure 7 presents the rotation poles and 95% confidence ellipses generated from the rotation parameters and misfit statistics. Between Paleocene and Eocene times (GEN – C22; ∼57–49 Ma) the progression of the poles is oriented southeastwards, and afterwards towards the north. The latter part of the progression resembles those in the qualitative solution of Gaina et al (2017) and the three-plate solution of *Gaina et al.* (2002). The new solutions and those of *Gaina et al.* (2002) mostly do not overlap at the levels of their respective 95% confidence regions. As we did for the EUR-NAM model, we attribute this to the combined effects of the order of magnitude increase in availability of flowline constraints to our method, and their orthodox treatment as chains of small circle segments. The new confidence ellipses are very much smaller than those determined previously in *Gaina et al.* (2009) two-plate solutions for the basin pairs north and south of the Jan Mayen fracture zone complex, and in some cases contained entirely within them.

The locations of the C6 and C13 poles are very similar to those of their counterparts in the EUR-NAM model, being contained within their 95% confidence ellipses. This observation confirms that plate divergence in the Labrador Sea, and with it independent motion of the Greenland plate, ended at the latest by C13 (33.16 Ma).

4.3 Greenland – North America Plate Divergence

Table 4 lists the sums of GRN-EUR and EUR-NAM rotation parameters, a set of five rotation parameters for Paleocene to Eocene (GEN/C25 to C18) GRN-NAM relative motions. Assuming Greenland earlier moved as part of a rigid Eurasian plate, additions of pairs of rotations from our EUR-NAM model yield a set of finite rotations for various periods, all ending at GEN/C25, and starting at times as far back as Late Cretaceous

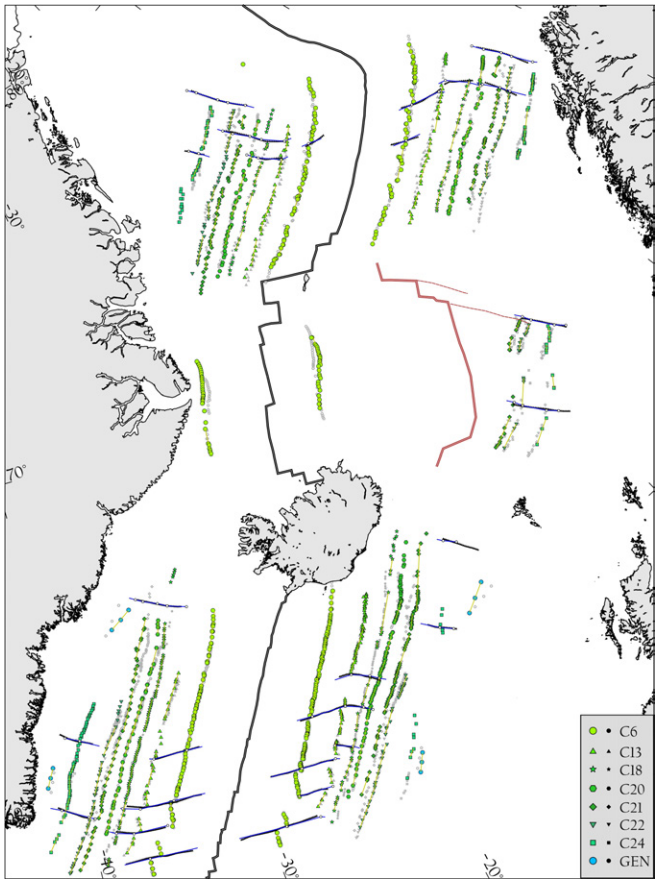

Figure 6 – Visual representation of fits in the GRN-EUR model. Coloured symbols: fixed isochron picks as in Supplementary Figure S1. Grey symbols: isochron picks after rotation in model. Yellow lines: great circle fitting targets based on isochron pick groupings. Small black triangles: accretionary flowline picks from Supplementary Figure S2. Blue lines: synthetic flowline segments designed to fit them. Double lines: modern plate boundaries from *Bird* (2003). Red lines: extinct Ægir Ridge and unused Jan Mayen fracture zone segments on its flanks, interpreted from satellite gravity (*Sandwell et al.*, 2014).

(C34; 83.64 Ma; Figure 8). By subsequent addition to the C25 rotation from Table 1, these enable us to generate a further eight sets of total finite rotation parameters for GRN-NAM divergence. These rotation parameters are also listed in Table 4. The poles are presented within estimated confidence ellipses in Figure 8, together with the poles of previous models (*Roest and Srivastava*, 1989; *Oakey and Chalmers*, 2012; *Torsvik et al.*, 2008; *Abdelmalak et al.*, 2019; *Longley et al.*, 2024). Lending some confidence to our results, it is possible to observe a good likeness between the progressions of previously published rotation poles and those of the new rotations for times after GEN/C25.

Gaina et al. (2002) did not list the quantitative post-C24 GRN-NAM solutions from their three-plate model. All of the previous GRN-NAM parameters represented in Figure 8 are derived from qualitative models, generated from seafloor spreading and other data in the Labrador Sea, and so lack formal uncertainty estimates to compare to ours. The uncertainty regions for GRN-NAM rotations are larger than those for the

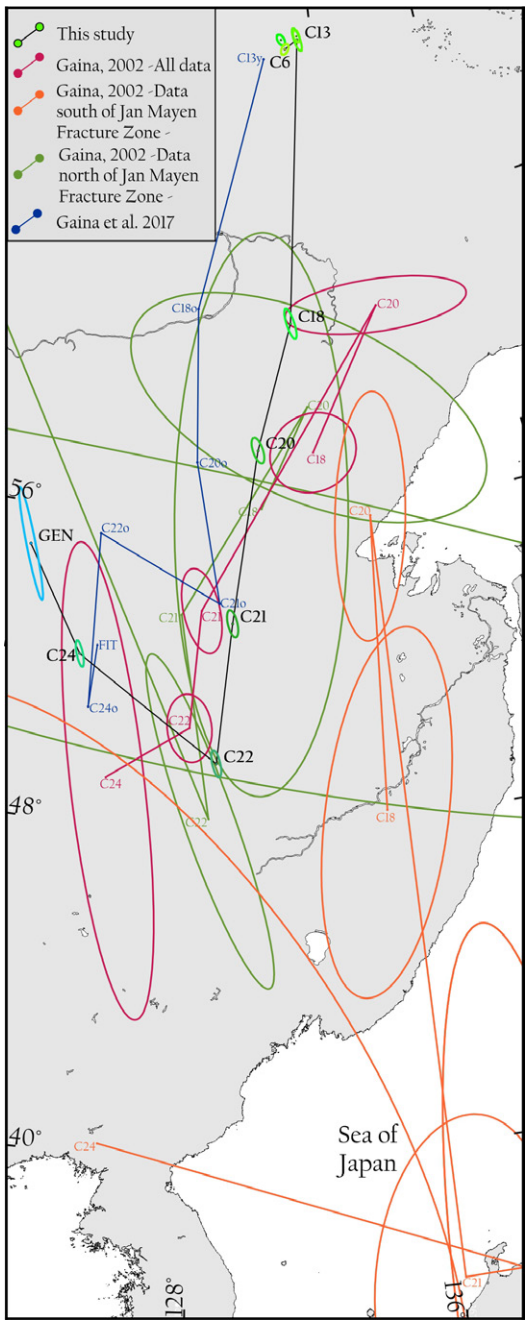

Figure 7 – Locations of the new GRN-EUR rotation poles and their 95% confidence ellipses, derived analytically from the covariances in Table 3. The colours of the ellipses correspond to those used for the picks in Figure 6. Four pole sets, three with graphically reproduced uncertainty ellipses, taken from two previous studies are shown for comparison and as described in the text. Poles and ellipses for C13 and C6 in the new EUR-NAM inversion (Table 2) are shown projected from the opposing hemisphere to enable comparison with their GRN-EUR counterparts, which are generated from a subset of the same data.

contemporary rotations in the two plate models for EUR-NAM and GRN-EUR motion. This is because they are each generated by convolution of pairs (for chrons C18-C24) or triplets (chrons GEN/C25-C34) of the estimated two plate model uncertainties. Despite the increased uncertainty, the larger number of modelled stages makes it possible to distinguish a broader U-shaped history of finite pole progression than is shown

Table 4 – Finite rotation parameters for GRN-NAM plate motion derived by summation of GRN-EUR and EUR-NAM parameters from Tables 2 and 3.

LAT	LON	ANG	CHRON
-60.68	103.78	1.35	C18
-59.75	86.52	1.90	C20
-60.01	85.16	2.85	C21
-61.18	85.22	3.59	C22
-41.25	66.11	3.29	C24
-23.77	49.34	3.13	GEN/C25
-17.29	32.50	3.35	C26
-15.54	20.02	3.77	C27
-21.29	18.19	4.18	C28
-25.40	16.86	4.39	C29
-31.41	16.60	4.89	C31
-48.08	17.91	6.71	C33
-50.87	16.01	7.46	C34

in previous studies (*Roest and Srivastava*, 1989; *Oakey and Chalmers*, 2012; *Torsvik et al.*, 2008; *Abdelmalak et al.*, 2019; *Longley et al.*, 2024).

Figures 9 and 10 present predictions of the timing and azimuth of plate divergence in the Labrador Sea made using the new GRN-NAM rotation parameters. Figure 9 does so using synthetic ridge-crest flowlines in the Labrador Sea. Figure 10 plots plate divergence rates and directions calculated for a point on the extinct mid-ocean ridge crest towards the southern end of the Labrador Sea, alongside rates determined in previous models. Figure 10 clearly illustrates how, as noted above, the determination of thirteen motion stages in the new model imparts far more detail than the three to nine stages covered by older ones.

The synthetic flowlines in Figure 9 are anchored at picks of C24, whose ages are more precisely known than the ages of points along the extinct ridge crest. This allows for a comparison between our model's predictions of dated age points and published magnetic reversal isochron interpretations (Gaina et al. 2002; Roest and Srivastava, 1989). The model consistently predicts seafloor isochrons in the post-C24 sequence that overlap with their observed equivalents within tight 95% confidence regions. Similarly, landwards of C24, the somewhat larger 95% confidence ellipses for the GEN/C25 and C26 markers reliably envelop picks of the C25 and C26 isochrons. The successful C25 prediction implies that our assumption of a C25 (57.1 Ma) age for GEN in the GRN-EUR model is indistinguishable, within error, from its true age. The C26 prediction implies that published picks of that isochron too are a reliable image of the Eurasian/North American mid-ocean ridge crest at 59.24 Ma.

The synthetic ridge-crest flowlines in Figure 9 can aso be compared to tectonic flowline fabric recorded in the Labrador Sea's satellite-derived gravity anomalies. In its post-C25 parts, the model presents open V-shaped model flowlines, each with a NNW-trending older arm, a NNE-trending younger arm, and an inflection at C22. Continuous fracture zones that might confirm

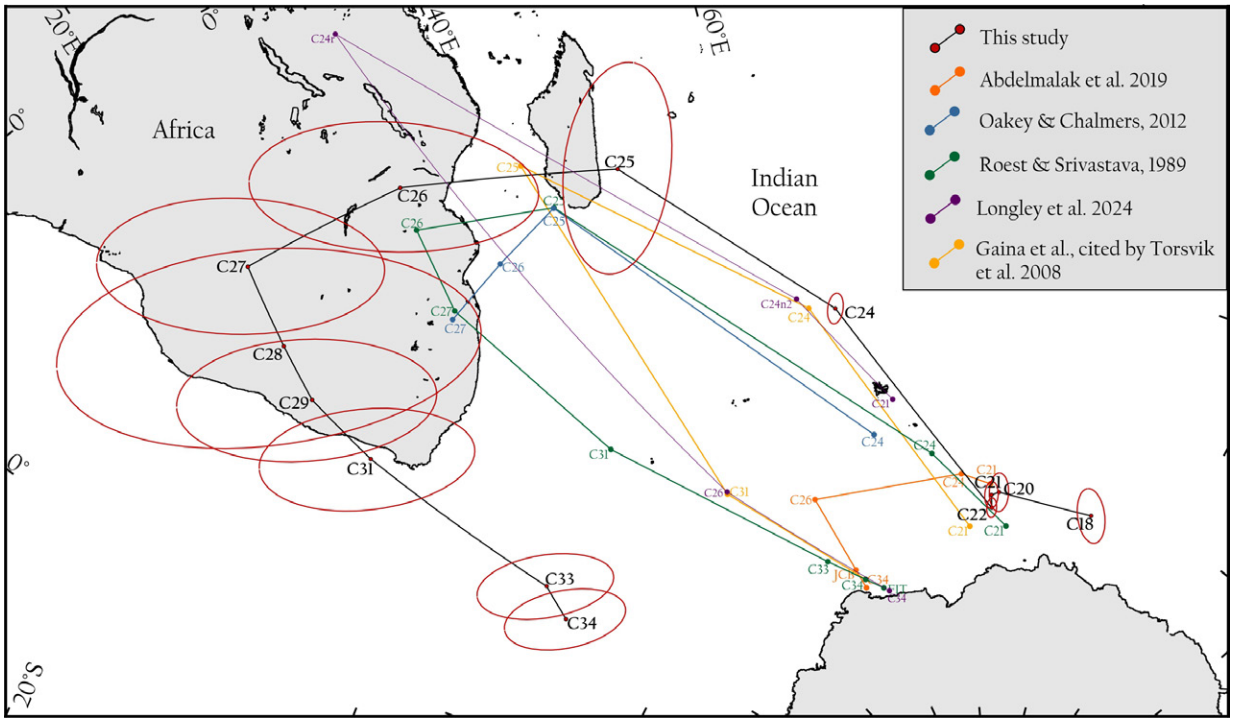

Figure 8 – Finite rotation poles for GRN-NAM motion, derived by composition of the circuit with the Eurasian plate using rotations from Tables 2 and 3, and compared to previous estimates derived directly from seafloor spreading and extended continental margin data from the Labrador Sea. 95% confidence ellipses are generated numerically by convolutions of the ellipses derived from Tables 2 and 3, and presented in Figures 5 and 7.

such a kinematic evolution are not observed in free-air gravity, but multiple linear lows over the rough basement surface of the axial region do hint at the presence of fracture zone-like valleys with the predicted orientations of the the two arms. The ENE-trending segments of pre-C25 flowlines closely match the lengths and orientations of the anomalies over the Cartwright and Julianhaab fracture zone segments. This latter match adds confidence to the notion that the earliest history of the Labrador Sea's opening happened between the North American and Eurasian plates, in spite of the lower formal confidence implied by the larger 95% estimated uncertainty regions for those times.

5 Discussion

5.1 Opening of the Labrador Sea

5.1.1 Between Continental Breakup and Seafloor Spreading

The NE-SW-oriented pre-Eocene flowlines segments in the pre-C25 parts of the Labrador Sea are constrained in the EUR-NAM model by rotations for C25, C26, C27, C28, C29, C31, C33, and C34. As noted already, picks of C25 and C26 there lie within the model's 95% uncertainty ellipses for the corresponding flowpoints (Figure 9). In contrast, the anomaly edges that Roest and Srivastava (1989) identified as isochron C31 lie variously within our model's C27 and C28 confidence ellipses, and all of the proposed (*Roest and Srivastava*, 1989) picks of C31 and C33 lie well inboard of the corresponding 95% confidence ellipses. Despite these mismatches, we have seen that the model accurately reproduces the azimuths of the old Cartwright and Julianhaab fracture zones. Taken together, these observations reinforce the conclusions of previous studies that the weak magnetic anomalies of the older parts of the Labrador Sea are not related to geomagnetic polarity reversals during the formation of 'normal' (~7 km thick) oceanic crust between diverging North American and Eurasian plates (*Chalmers*, 1991; *Chalmers and Laursen*, 1995; *Keen et al.*, 2018; *Chian et al.*, 1995). More specifically, one of those studies (Keen et al. 2018) used seismic data to identify a 'proto-oceanic domain' of thin and variable oceanic crustal thicknesses and, further landwards still, a basement of hyperextended continental crust and serpentinized and exhumed mantle that may or may not be of subcontinental origin. Those authors dated the proto-oceanic crust to chrons C31-C27 (68.4-62.5 Ma in our chosen timescale). In contrast, our results suggest this crust formed later and somewhat faster, between C28 and a time during the reversed polarity part of chron C26 (i.e. at ~64.7-60 Ma). Apart from the different timing, our model is fully consistent with the idea that the proto-oceanic setting was succeeded by a magmatic divergent plate boundary in the Labrador Sea. The linear magnetic anomalies marginwards of C26 in the Labrador Sea are unlikely to be useful as plate edge isochrons for kinematic reconstructions unless they can be dated independently of models built using magnetic polarity reversal timescales.

Figure 10 shows how plate divergence predicted for the Labrador Sea by our model starts relatively slow at 6-10 km/Myr (expressed as a seafloor spreading half rate). An acceleration is underway by C31 (~68 Ma)

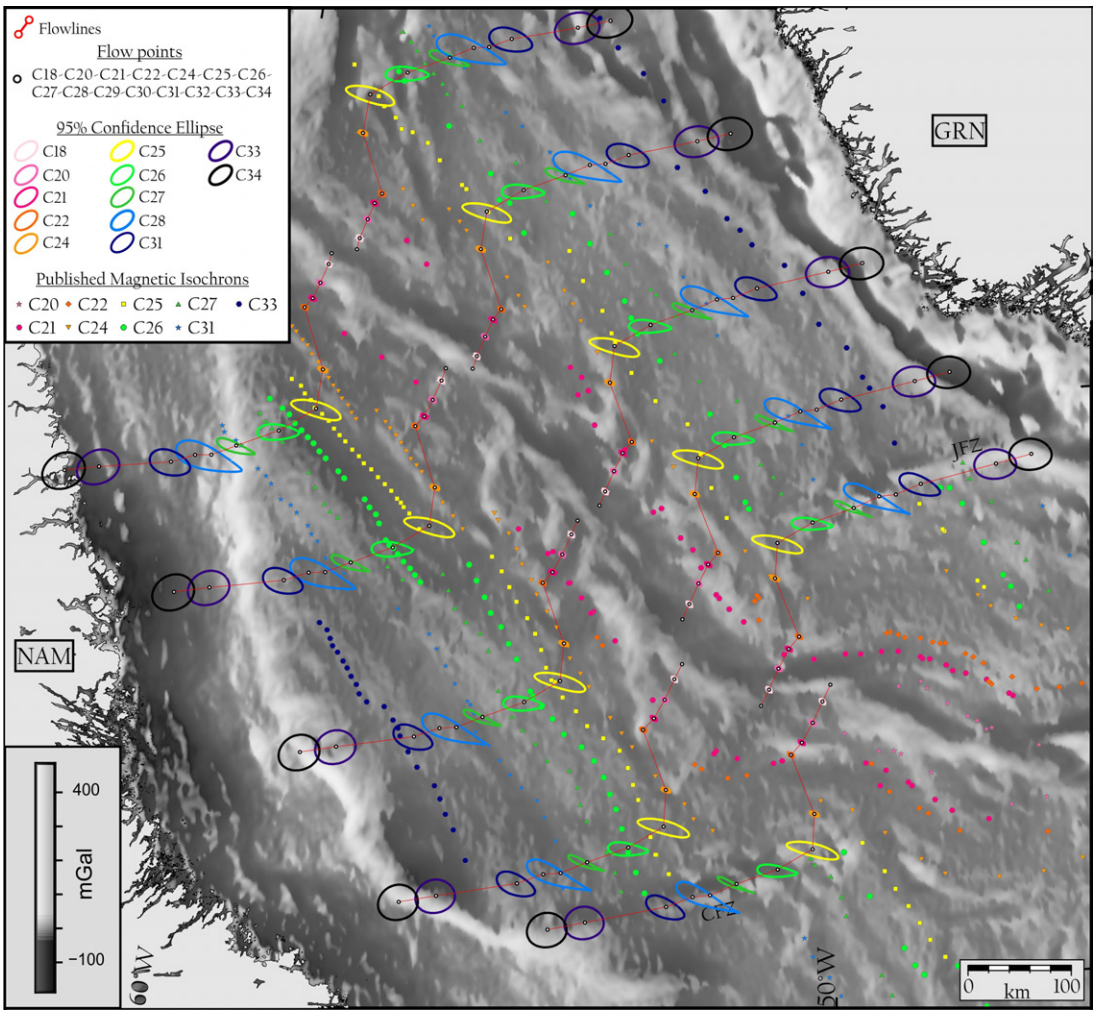

Figure 9 – Synthetic GRN-NAM ridge crest flowlines for the Labrador Sea generated using the finite rotations in Table 4 and seed points anchored on published picks of chron C24. 95% confidence regions around selected dated points along the flowlines are calculated numerically using the GRN-EUR and EUR-NAM confidence estimates derived from Tables 2 and 3. Coloured symbols show previous picks of magnetic reversal isochrons in the region, archived from various sources (*Seton et al.*, 2014). Background: free air gravity from *Sandwell et al.* (2014). CFZ, JFZ: Cartwright and Julianhaab fracture zones.

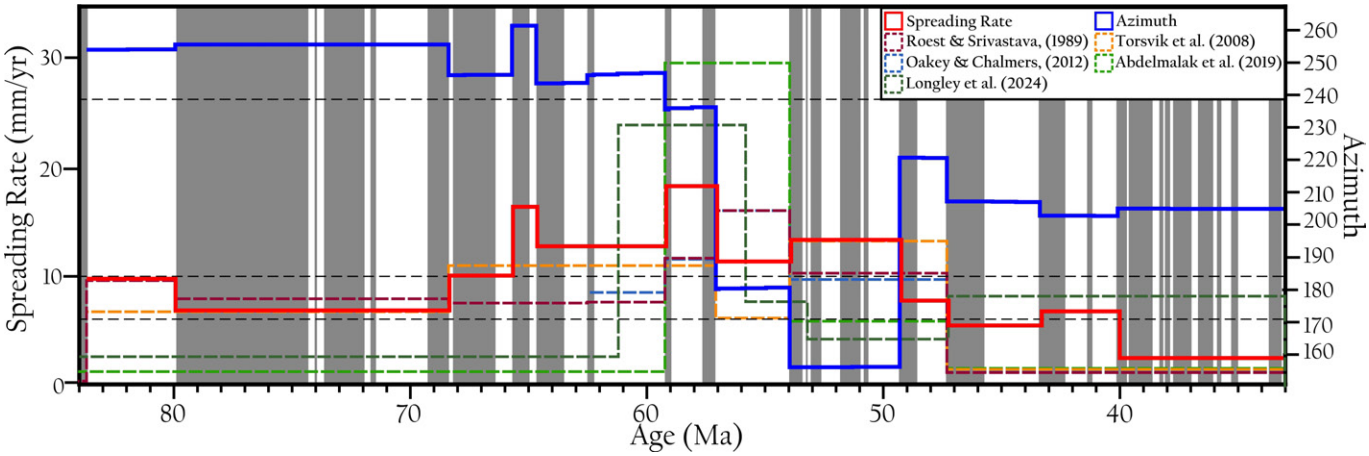

Figure 10 – GRN-NAM Plate divergence rates (represented by seafloor spreading half-rates) and azimuths predicted by the rotations in Table 4 for a point in the central Labrador Sea. Dashed lines mark the approximate transitions between ultra-slow, slow, and intermediate seafloor spreading half rates.

and continues until reaching ~18 km/Myr by C26-C25. After this, and accompanying the onset of focussed plate divergence east of Greenland, rates steadily decline until the eventual extinction of the plate boundary in the Labrador Sea at or before C13. Spikes in the divergence rate appear at chrons C29 and C26. The C29 spike, appearing as a near-100% increase over the pre-C29 spreading rate, is closely reminiscent of contemporaneous spikes observed in high resolution models for multiple plate pairs worldwide, which are best

understood as artefacts of a timescale error (*Pérez-Díaz et al.*, 2020). The C26 spike is not observed globally. It marks an inflection between periods of long-term acceleration and deceleration in plate divergence rates. The inflection accompanies inaugural motion of the independent Greenland plate. The C26 spike therefore is likely to be a real feature of Greenland's divergence from North America. Its true height and duration will be responsive to errors in the date attributed to GEN, at its younger end, that exist below the sensitivity of our model.

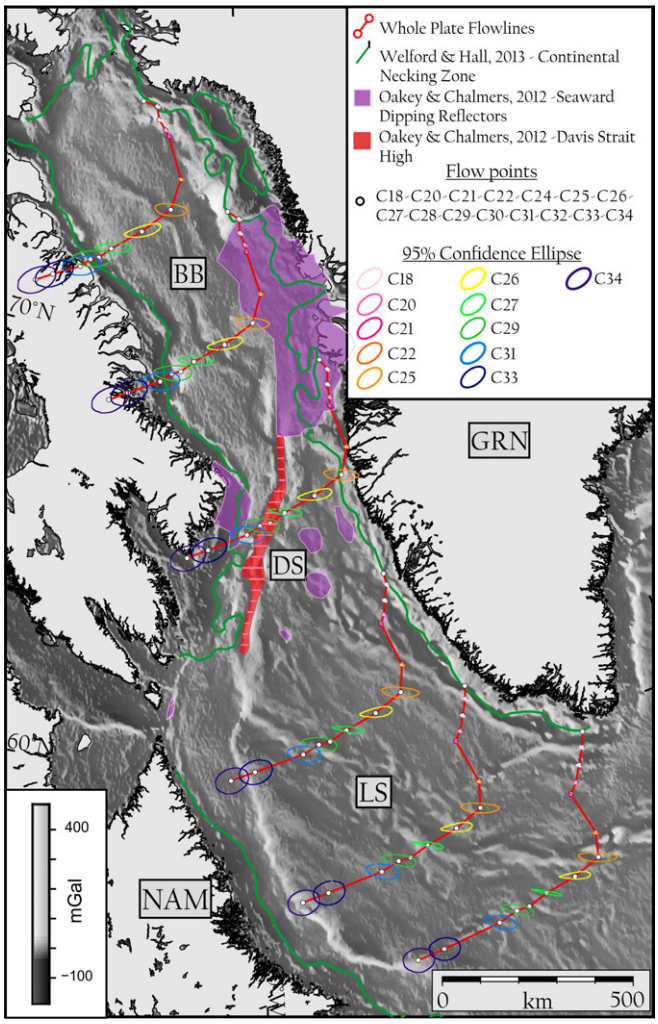

Figure 11 – Whole plate motion flowlines for Labrador Sea (LS), Davis Strait (DS) and Baffin Bay (BB), seeded at points on the west Greenland continental necking zone (20 km crustal thickness contour from gravity inversion by *Welford and Hall*, 2013). 95% confidence regions around selected dated points along the flowlines are calculated numerically using the GRN-EUR and EUR-NAM confidence estimates derived from Tables 2 and 3. The regions for post-C25 flowpoints are plotted, but difficult to discern because they are very small. Background: free air gravity from *Seton et al.* (2014).

Assuming the pre-C26 seafloor to consist solely of newly created areas of 'proto-oceanic' crust and mechanically exhumed oceanic mantle (*Keen et al.*, 2018), flowlines can be used to estimate an earliest possible time for continental breakup by observing where they cross the zones of crustal necking that herald its onset. The ridge crest flowlines in Figure 9 are not ideal for this task owing to the effects of asymmetric seafloor spreading, whose effect is to shift possible anchor points on the paleo-ridge crest or individual isochrons relative to the extended continental margins. To avoid these effects, we plot a set of whole plate motion flowlines for the Eurasian plate that emanate from anchor points on the Greenland necking zone, approximated by the 20 km crustal thickness contour of *Welford and Hall* (2013) (Figure 11). In the Labrador Sea south of 60°N, three flowlines suggest EUR-NAM continental necking pre-dates chron C34 (83.64 Ma; earliest Campanian). Linear extrapolations of these three flowlines to the Canadian-side necking zone potentially date necking and the onset of breakup to 88-91 Ma. A preceding period of slow extensional strain can be interpreted, on the basis of biostratigraphic ages on growth strata, to have started as early as 140 Ma and ended by ~99 Ma (*Dickie et al.*, 2011) or, on the basis of radioisotopic dates on volcanic strata, as late as 93 Ma (*Knudsen et al.*, 2020). The Labrador Sea thus seems to follow the previously observed pattern of continuous long periods of lithospheric thinning that culminate in continental breakup in short lived continental necking episodes (*Brune et al.*, 2016). The time lag between necking and the occurrence of plume-related volcanism in the northern Labrador Sea and north of it (~61 Ma *Dickie et al.*, 2011; *Chalmers and Pulvertaft*, 2001; *Srivastava*, 1978; *Graham et al.*, 1998; *Clarke and Beutel*, 2020) reinforces previous conclusions that the onset of continental breakup in the Labrador Sea was a response to the evolving balance of plate boundary stresses, rather than mantle plume activity (*Peace et al.*, 2017).

5.1.2 Oblique Slip Accommodating Very Oblique Seafloor Spreading? Eocene Labrador Sea

Figures 8-11 show that the onset of Greenland plate motion at ~57 Ma in our models leads to a dramatic change in plate divergence azimuth in the Labrador Sea, which between the C27-C26 (~63-59 Ma) and C24-C22 (~55-49 Ma) stages rotates counterclockwise by nearly 90°. Magnetic isochrons from before and after the rotation (C26–C22; 58.96–48.57 Ma) show that much of the ridge crest maintained a constant orientation, leaving it aligned nearly parallel to the new azimuth of plate divergence (Figure 9). Worldwide, there are currently no long segments of active mid-ocean ridge with such strong obliquity to the normal to plate divergence; the typical range is instead up to ~25° (*Seton et al.*, 2020). Seismological studies at ridges near the extremes of this range show that oblique-slip earthquakes and faults are rare, and that the neotectonic zones are instead populated by en-echelon sets of strike-slip faults and short-lived normal faults whose strikes run approximately perpendicular to the azimuth halfway between the plate divergence azimuth and the normal to the ridge crest (*Fournier and Petit*, 2007). In the Labrador Sea after GEN/C25, the strike of such normal faults, if they developed, should have been either south or east. The presence of

normal faults with these strikes cannot be confirmed with the sparse available seismic reflection data, which typically do not reveal basement structures in much detail (e.g., *Delescluse et al.*, 2015; *Hinz et al.*, 1979). Gravity anomalies, in contrast, suggest the presence of 50-90 km-long abyssal hills parallel to the fossil ridge crest and magnetic isochrons in the C24-C22 aged crust on both flanks of the ridge (Figure 9). At slow-spreading ridges, abyssal hill fabric is related to the action of normal faults (*Goff*, 2023). Hence, it seems possible that large normal faults originally formed at the Labrador Sea ridge before chron C25, and may have started to act in oblique and later very oblique slip between chrons C25 and C22. Faults like these may thus occur more commonly at high-obliquity spreading centres than can be extrapolated from studies of active, moderate-obliquity, examples.

Magnetic reversal isochrons younger than C21 (<47.4 Ma) are only observed in the southeasternmost parts of the Labrador Sea. In our model, plate divergence rates drop slightly, but crucially, into the range (10.0-6.0 km/Myr half-rate) within which the features of ultra-slow seafloor spreading ridges become established (*Dick et al.*, 2003) for the first time just prior to C21 (Figure 10). This is consistent with the near absence of post-C21 isochrons, because ultra-slow spreading is associated with accommodation of plate divergence by widespread mechanical, rather than igneous, processes, leaving a thin and discontinuous basalt magnetic carrier layer, as observed in the axial region of the Labrador Sea (*Srivastava and Keen*, 1995; *Delescluse et al.*, 2015). Magnetic isochrons near the South Greenland Triple Junction may date these processes to have endured until around chron C13 (33.16 Ma) (*Oakey and Stephenson*, 2008). Consistent with this, our GRN-EUR and EUR-NAM models sum to zero for post-C13 GRN-NAM motion, within their respective uncertainties (cf. Figure 7).

5.2 Davis Strait

The whole-plate flowline plotted for the Davis Strait region in Figure 11 crosses the necking zone on the Labrador margin at or slightly before chron C31, suggesting breakup there by 68.4 Ma. The alignment of the Greenland and Labrador margins prior to breakup is considerably tighter than that of Longley et al. (2024) and does not accommodate their interpretation of 18-26 km thick crust in Davis Strait in terms of a partially detached microcontinent.

Following C31 and until C24, our model resolves ∼320 km of plate divergence oriented NE-SW, strongly oblique (∼40°) to the strikes (NNE) of the shelf edges bounding the strait. With this obliquity, the divergence would have produced a ∼206 km wide and ∼245 km long corridor of extended continental and transitional and/or oceanic crust between the shelves. Occurrences of seaward dipping reflectors on both sides of the strait suggest that at least some of the development of this corridor played out subaerially. Between them, a prominent basement and seafloor high, the Davis Strait High (Figure 11), runs NNE along the floor of the strait. This feature strikes parallel to the orientation of relative plate motion during the model's C25-C24 stage, suggesting it may have originated as a transform fault on the young mid-ocean ridge at that time. Following C24, the whole plate flowlines show a period of ∼250 km NNW-oriented relative motion, composed of components with lengths of ∼215 km parallel to the axis of the high, and ∼125 km perpendicular to it. The latter component implies around 60% shortening of the pre-GEN/C25 aged crustal corridor along an active transpressional plate boundary segment whose remnants today are to be found at the Davis Strait High.

Our finding of oblique post-C24 convergence in Davis Strait reinforces those of previous plate kinematic models (*Oakey*, 2005; *Oakey and Chalmers*, 2012; *Roest and Srivastava*, 1989; *Torsvik et al.*, 2008; *Abdelmalak et al.*, 2019), interpretations of geophysical and geological data (*Chalmers and Pulvertaft*, 2001; *Suckro et al.*, 2012; *Gion et al.*, 2017; *Peace et al.*, 2018), and numerical models (*Farangitakis et al.*, 2020). Our model (Figure 11) further suggests that the obliquity of the collision may have rotated over time, easing slightly after C22. The overall history of oblique divergence followed by oblique convergence across Davis Strait prompts us to attribute uplift of the Davis Strait High (Figure 2) and thrusting and folding in the Ikermiut Fault Zone to reactivation of pre-existing (pre-GEN/C25) extensional and transform fault structures (*Piepjohn et al.*, 2016; *Dalhoff et al.*, 2006; *Gregersen and Bidstrup*, 2008). The complementary strike-slip component is recorded in onshore data by evidence for left-lateral motion within the Itilli Fault Complex east of the Davis Strait High (*Peace et al.*, 2018; *Sørensen et al.*, 2017).

5.3 Baffin Bay

The whole plate flowlines in Figure 11 cross the Baffin Bay necking zone between chrons C31 and C28 in the south (∼68-65 Ma), but at around C28 further north. These ages suggest continental breakup at a focussed plate boundary zone started as much as 25 Myr later in Baffin Bay than in the Labrador Sea. They are also consistent with the idea that the North American-Eurasian plate boundary propagated northwards through the region during late Cretaceous and earliest Paleogene times. Isolated basins over <20 km-thick continental crust on the Greenland margin (*Welford and Hall*, 2013), widespread normal faulting and scattered late Cretaceous and Paleocene alkaline and tholeiitic volcanism northwest of Baffin Bay (*Tegner et al.*, 2011) are consistent with the corollary expectation, that earlier plate divergence was taken up by unfocussed continental extension.

Between its necking zones there is no consensus on the presence and identifications of magnetic anomaly isochrons in Baffin Bay (*Oakey and Chalmers*, 2012; *Suckro et al.*, 2012), leading some to question the presence of oceanic crust (*Reid and Jackson*, 1997). However, seismic refraction profiles have repeatedly demonstrated typical oceanic crustal P-wave velocity

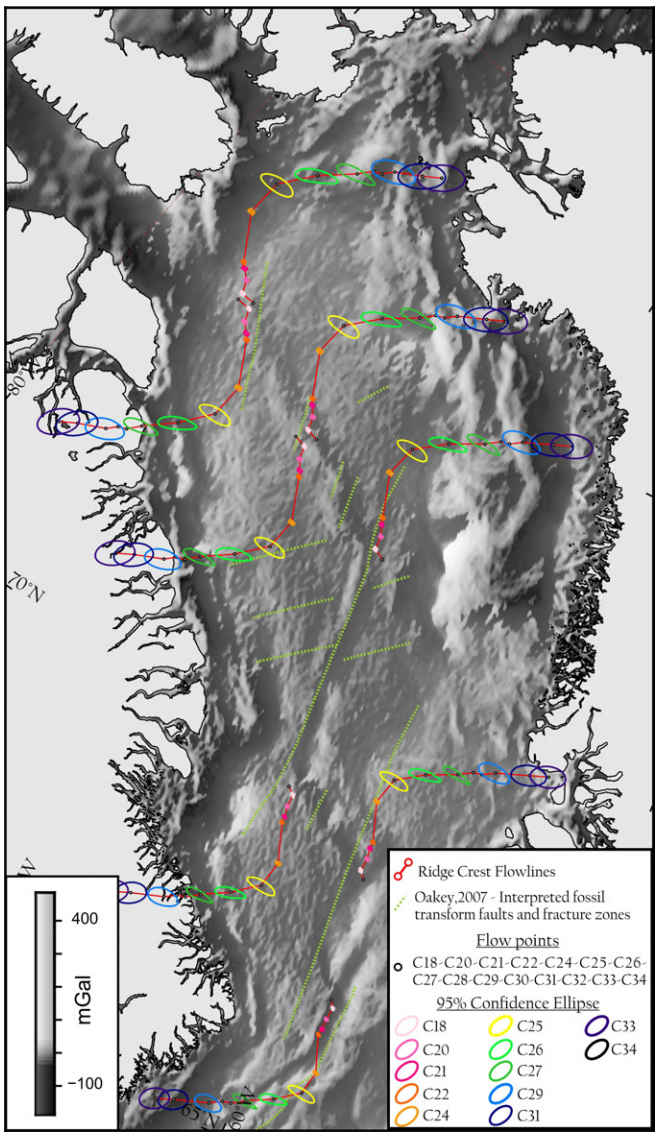

Figure 12 – Synthetic GRN-NAM ridge crest flowlines for Baffin Bay generated using the finite rotations in Table 4 and seed points anchored on published picks of chron C24. 95% confidence regions around selected dated points along the flowlines are calculated numerically using the GRN-EUR and EUR-NAM confidence estimates derived from Tables 2 and 3. Dashed lines are previously interpreted FZs and fossil transforms, based on offsets of undated magnetic anomaly isochorns (*Chalmers and Oakey*, 2007). Background: free air gravity from *Sandwell et al.* (2014).

profiles (*Funck et al.*, 2012; *Suckro et al.*, 2012; *Reid and Jackson*, 1997; *Altenbernd et al.*, 2014) and altimetry-derived free-air gravity data have revealed a possible buried extinct median valley offset by fossil transform faults, and flanked by fracture zones (*Oakey and Chalmers*, 2012; *Chalmers and Pulvertaft*, 2001; *MacLeod et al.*, 2017; *Jagoutz et al.*, 2007; *Whittaker and Hamann*, 1997). Our model provides a detailed new context with numerical confidence estimates within which to understand the tectonic development of these features (Figure 12). Ridge-crest flowlines seeded at the shoulders of the interpreted median valley depict pre-Eocene NE-SW plate divergence, perpendicular to NW-SE striking normal faults within the bay's continental margins (*Gregersen et al.*, 2013) and parallel to fracture zones interpreted from offsets of the basin's indistinct magnetic anomalies (*Chalmers and Oakey*, 2007).

The model resolves a period of N-S to NNW-SSE oriented plate divergence between the onset of Greenland Plate motion at GEN/C25 (~57 Ma) and C18 (40 Ma). This too is consistent with the orientations of fracture zones and large transform faults associated with the interpreted median valley (*Sandwell et al.*, 2014). After C18, the model shows N-oriented motion that is parallel to the trend of the interpreted extinct ridge at its southern end, but further north obliquely convergent with it. This implies the mid-ocean ridge in northern Baffin Bay would have ceased to accommodate plate divergence around 7 million years earlier than previously suggested by extrapolation from the Labrador Sea (*Oakey and Chalmers*, 2012; *Hosseinpour et al.*, 2013). Existing plate models (*Roest and Srivastava*, 1989; *Oakey and Chalmers*, 2012; *Torsvik et al.*, 2008; *Abdelmalak et al.*, 2019) suggest in contrast that active seafloor spreading at the mid-ocean ridge in Baffin Bay occurred synchronously with Eurekan compression of the neighbouring continental margin (*Altenbernd et al.*, 2014; *Gregersen et al.*, 2013). Instead of this complexity, our model shows a diachronous north-propagating transition between plate divergence and convergence at times after C18. This is consistent with the seismic observations of NW trending compressional structures very close to the extinct mid-ocean ridge (*Harrison et al.*, 2011) and middle Eocene (post-C22, 48.62 Ma) inversion structures in the Melville Graben (*Knutz et al.*, 2012), and of a hiatus in the Hellefisk-1 well (*Nøhr-Hansen*, 2003).

Late Cretaceous to Paleocene EUR-NAM stage rotations (Table 5; Figure 13) occur about poles that require plate divergence rates to have been ~5% slower in Baffin Bay than further south in the Labrador Sea. This gradient does not support an interpretation of the contrasting presence of seaward dipping reflectors in Davis Strait and southern Baffin Bay and exhumed mantle further south in the Labrador Sea (*Oakey and Chalmers*, 2012; *Keen et al.*, 2018, Figure 11) in terms of variable plate divergence and mantle upwelling rates. Furthermore, plate divergence rates calculated from the model for the time (C27; 62.52 Ma) and location of seaward dipping reflector formation are relatively slow in global terms, at ~15 mm/yr (Figure 10). These observations all suggest that the seaward dipping reflectors are rather products of interaction between the young plate boundary and the Iceland mantle plume, consistent with the presence of Selandian (61 Ma) picrites along the southwest Greenland margin (*Dickie et al.*, 2011; *Chalmers and Pulvertaft*, 2001; *Srivastava*, 1978; *Graham et al.*, 1998; *Clarke and Beutel*, 2020).

Figure 13 hints at a general tendency for southwards migration of late Cretaceous and Paleocene stage poles, ahead of the propagating tip of the young divergent boundary in the Labrador Sea. The migration of the pole locations accelerates considerably and becomes statistically significant by the stage between chrons C27 and C26, accompanying the effusion of basalt

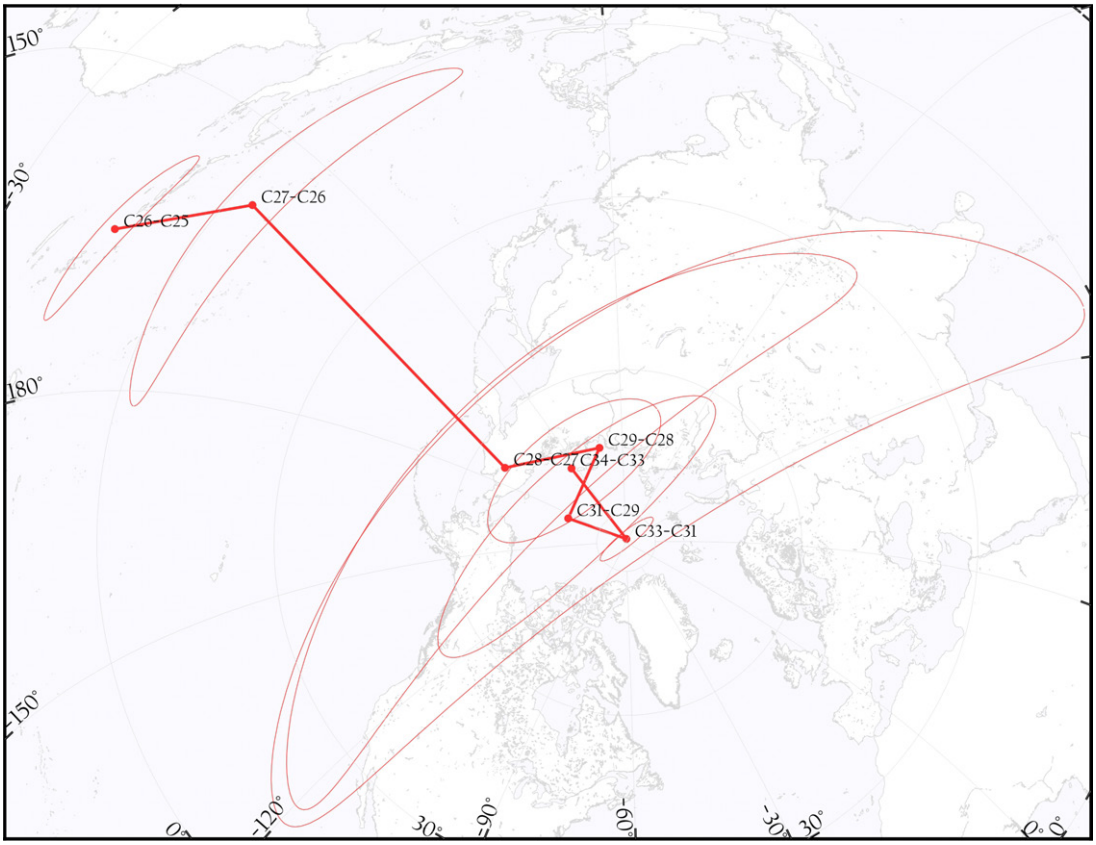

Figure 13 – Locations of stage poles for EUR-NAM motion prior to independent motion of the Greenland plate. Poles calculated from the finite rotation parameters in Table 2. Confidence ellipses generated numerically using the 95% confidence regions derived from Table 2. The very large size of the ellipses is an expected result of the small rotation angles about the stage poles.

Table 5 – Stage rotation parameters for EUR-NAM plate motion derived by summations of parameters from Table 2.

LAT	LON	ANG	STAGE
-12.51	164.24	0.98	C26-C25
3.53	157.56	0.86	C27-C26
65.61	173.68	0.58	C28-C27
72.96	132.91	0.39	C29-C28
79.28	-176.07	0.69	C31-C29
89.37	111.41	2.47	C33-C31
74.13	152.88	0.84	C34-C33

SDRs, picrite eruptions, and focussing of the plate boundary in Davis Strait and Baffin Bay. There is, however, no accompanying change in the acceleration or azimuth of GRN-NAM plate divergence (Figure 10). We interpret the first of these associations as a signal of the localization and stabilization of a long segment of the plate boundary by the arrival of plume related melt into the mantle and crust beneath Davis Strait and southern Baffin Bay at C27 and with a globally observed tendency for plumes and divergent boundaries to migrate and/or localize near one another and afterwards maintain proximity (*Whittaker et al.*, 2015). The second association is consistent with the previous observations that demonstrate an absence of large plate velocity changes in response to plume arrivals at the base of the lithosphere in other settings (*Pérez-Díaz et al.*, 2020; *Eagles*, 2024).

5.4 Plate Motion and Plate Boundary Deformation North of Greenland

A recent GPlates model-based study (*Gion et al.*, 2017) considered development of the collisional GRN-NAM plate boundary north of Greenland in its major-plate motion context. For this context, the publicly available version of the model used GRN-NAM rotations from *Hosseinpour et al.* (2013) for its 'full fit' and *Torsvik et al.* (2008) at all other times, and EUR-NAM rotations from *Gaina et al.* (2002) (note that *Gion et al.* (2017) cite different rotation sources). For the collisional boundary, it defined a set of rigid body rotations between numerous previously defined small blocks, and a mesh based procedure to enable determinations of non-rigid deformation in the evolving spaces between the blocks. The authors found that the sum of the rigid block rotations (and, hence, of non-rigid deformation within the meshes) broadly matches the framing context.

Schouten and van Hinsbergen (2021) reviewed an approach to generating plate tectonic scenarios from constraints preserved in continental collision zones, like that taken in part of the *Gion et al.* (2017) study. They stressed how the loss, non-exposure, and reworking that geological markers can be expected to suffer in such settings means they must be expected at best to deliver minimum estimates of plate motion. Added to this limitation, *Gion et al.* (2017) defined their rigid blocks much as had first been done by *Lawver et al.*

(1990), using fault trends interpreted from field studies summarized by *de Paor et al.* (1989). These same blocks are widely used in global reconstruction studies (e.g., *Müller et al.*, 2008; *Seton et al.*, 2012; *Matthews et al.*, 2016; *Müller et al.*, 2019) that have been taken as the contexts for detailed regional interpretations (e.g., *Tegner et al.*, 2011; *Døssing et al.*, 2013; *Japsen et al.*, 2023). Since *de Paor et al.* (1989), however, the results of new fieldwork have served to begin disentangling the records of the Eurekan and older (Paleozoic) Ellesmerian or Innuitian orogeny that both affected the island. In particular, the idea that Eurekan sinistral strike-slip motion occurred distributed on faults throughout the island, which *de Paor et al.* (1989) tested but could not unequivocally support, has become more confidently acceptable (e.g., *Piepjohn et al.*, 2016; *Piepjohn and von Gosen*, 2018).

In this section, we describe an updated GPlates model (see supplementary material) for the late Cretaceous and Cenozoic collision zone north of Greenland. To build this model, we assumed that the collision zone first came into existence following focussing of relative plate motion into the neighbouring northern part of Baffin Bay around chron C28 (∼65 Ma; Figure 11). This is consistent with evidence from scattered alkaline volcanism for the pre-65 Ma action of a distributed extensional plate boundary zone in the Canadian Arctic archipelago, Ellesmere Island, and northern Greenland (e.g., *Tegner et al.*, 2011). For the collision zone, we updated the number and boundaries of rigid blocks on Ellesmere Island on the basis of conclusions from post-1980s fieldwork, as summarized by *Piepjohn et al.* (2016); *Piepjohn and von Gosen* (2018). We defined the major plate motion context on the basis of the new EUR-NAM and GRN-NAM rotations of Table 2 and 4 and applied motions calculated from discrete stages amongst those rotations to our reinterpreted Ellesmere Island blocks. To do this, we noted how our rotations imply three distinct consecutive stages of GRN(EUR)-NAM relative motion, each of which is recapitulated in published strain sense and azimuth estimates for individual large faults and fault systems in the islands north of Greenland. Following these similarities, we assigned relative motions to discrete tectonic blocks between some of the faults in such a way that the blocks moved plausibly with respect to their neighbours. We did not attempt to closely match the magnitudes of published estimated strain vectors on any of the individual faults in view of the fact that these are unlikely to be complete records of relative plate kinematics . We ensured to use all available stage rotations once only, so that the sum of relative block rotations equals the framing set of main plate rotations, which is much closer to complete. The new model does not define any meshes for determinations of non-rigid displacements between its blocks.

5.4.1 Nares Strait

Diverse pre-kinematic markers from Ellesmere Island and northern Greenland suggest that Paleocene and later relative movements between Greenland and North America were accommodated by sinistral strike-slip motion parallel to the narrow seaway northwest of Greenland, Nares Strait (e.g., *Dawes and Kerr*, 1982; *Harrison*, 2004). The 61-58 Ma period also saw alkaline volcanism in Nares Strait (*Estrada et al.*, 2009), implying some degree of Paleocene continental extension there. Seismic reflection and magnetic evidence for the presence of pull-apart basins along the strait (e.g., *Tessensohn et al.*, 2004; *Harrison et al.*, 2011; *Ehrhardt et al.*, 2016) most likely confirm a transtensional setting for this extension. Estimates of the magnitude of strike-slip displacement across the strait vary enormously, between 0 and >215 km. Although the largest of these offsets is estimated using one of the best quality constraints, most of the others cluster in the range 50–100 km (*Saalmann et al.*, 2005; *Harrison*, 2004; *Tessensohn et al.*, 2004; *Gilotti et al.*, 2018). The clustered values are strongly at odds with the idea that the strait may have taken up all of the 300-400 kilometres of relative GRN-NAM motion that can be surmised from studies of the Labrador Sea and Baffin Bay. This disagreement is the central

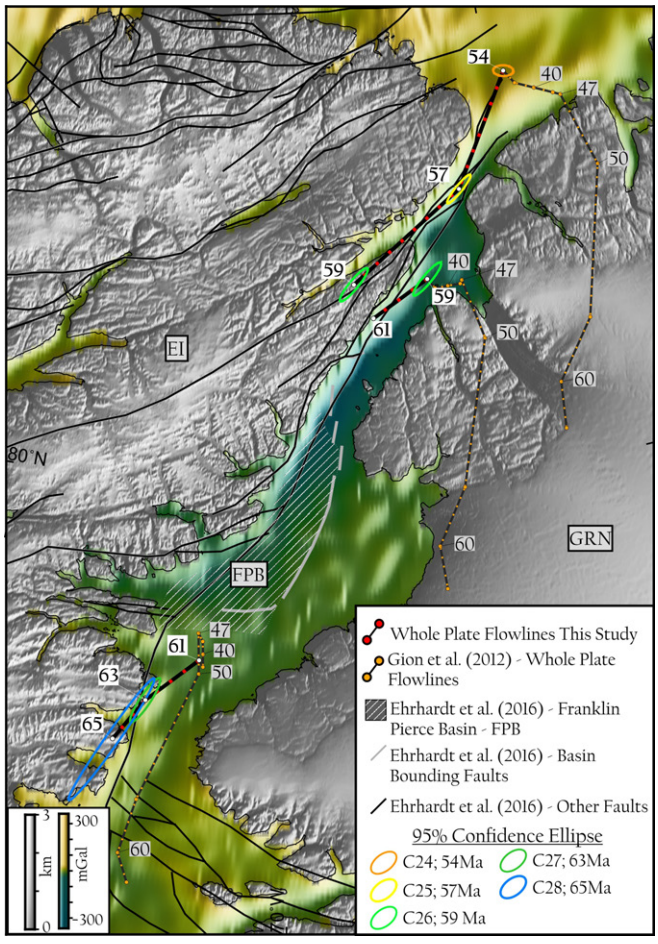

Figure 14 – GPlates model motions (black/red, this study; black/orange, Gion et al. 2017; selected flowpoints with equivalent chronostratigraphic ages, in Ma, to aid comparison) of Greenland with respect to fault-bounded blocks of Ellesmere Island across Nares Strait. 95% confidence regions around selected dated points along the flowlines are calculated numerically using the EUR-NAM confidence estimates derived from Table 2. Background: SRTM topography onshore; *Gaina et al.* (2011) gravity offshore (blue colours towards negative, yellow towards positive).

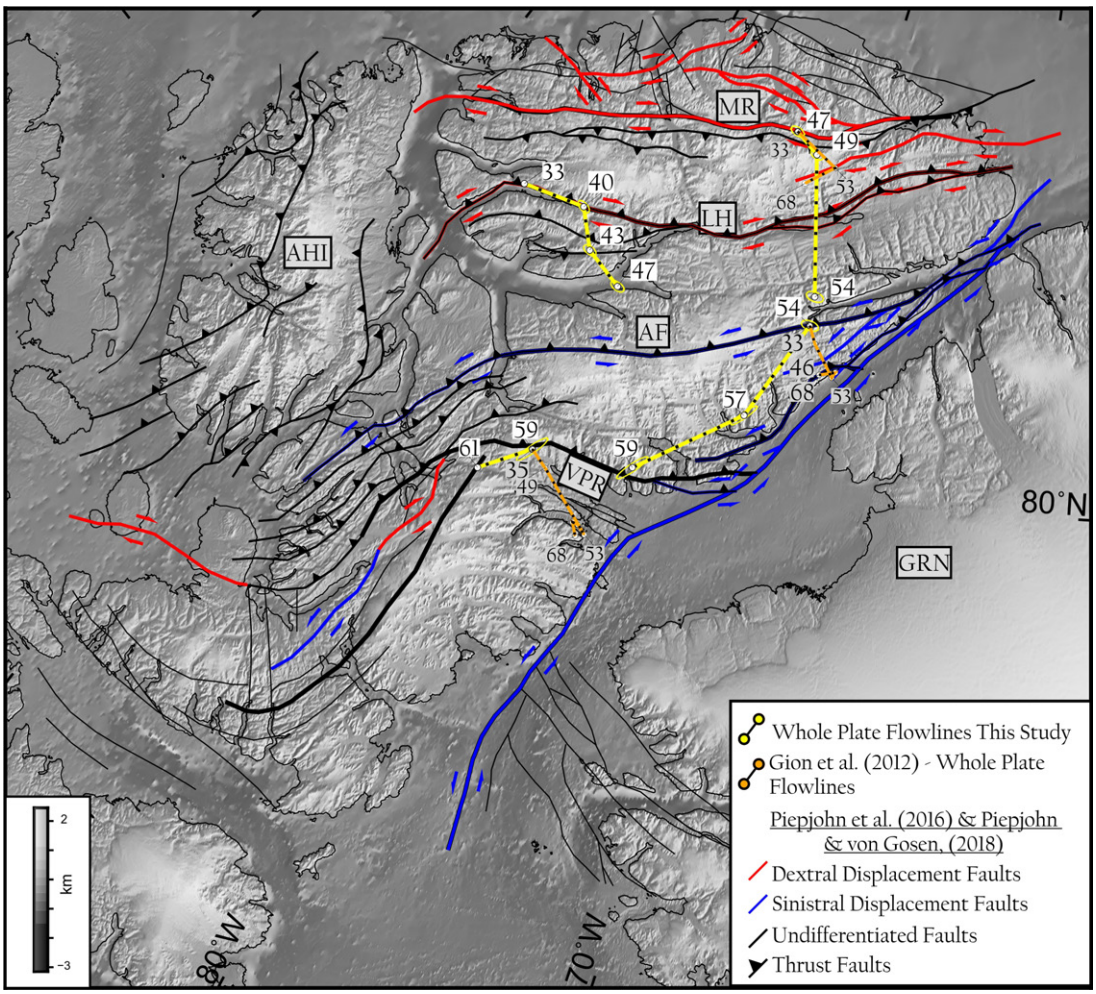

Figure 15 – GPlates model motions (yellow, this study; orange, *Gion et al.* (2017); selected flowpoints with equivalent chronostratigraphic ages, in Ma, to aid comparison) across named block-bounding faults in Ellesemere Island. Note that the 95% confidence regions around our model's flowpoints are plotted, but very small. Blue: faults with sinistral displacements. Red: faults with dextral displacements. Barbed black lines: thrust and reverse faults. Unadorned lines: undifferentiated faults. All faults from *Piepjohn et al.* (2016) and *Piepjohn and von Gosen* (2018). Background: SRTM topography.

subject of a longstanding debate about the existence and importance of the so-called Wegener Fault, a proposed focused GRN-NAM plate boundary segment in Nares Strait (e.g., *Harrison*, 2004; *Tessensohn et al.*, 2004; *Rasmussen and Dawes*, 2011).

Gion et al.'s (2017) plate motion study depicts sinistral motion all along Nares Strait at 65-47 Ma (Figure 14). Varying according to which individual block of Ellesmere Island is involved, the modelled amount of motion with respect to Greenland increases eastwards from 180 km to 240 km, always greater than suggested by the majority of field observations but consistent with the chosen framework of major plate motions. This motion accompanies a large convergent cross-strait component, which increases eastwards in magnitude from ∼40 km to ∼120 km. The convergence is inconsistent with *Estrada et al.*'s (2009) evidence for 61-58 Ma extension from alkaline volcanism and the presence of pull-apart basins along the floor of Nares Strait. Motion after 47 Ma is lightly divergent (∼20 km) in the west and strongly convergent (∼30-50 km) in the east of the strait.

Our new model predicts sinistral EUR-NAM motion parallel to Nares Strait in the C28-C24 (∼64.5-54 Ma) period (Figure 14). We apply this motion piecewise to the blocks of Ellesmere Island that bound Nares Strait, implying sinistral strike-slip motion between them and along different parts of the strait in Paleocene times. Between Greenland and the eastern part of Ellesmere Island, this motion amounts to 80 ± 65 km, including a ∼25 km divergent component. Further east, between Judge Daly Peninsula and Greenland, motion is 45 ± 18 km, sinistral, and similarly lightly divergent. These motions are broadly consistent with the majority of geologically-based estimates of strike-slip along the strait (*Harrison*, 2004). Further east, where there are fewer geological offset markers of any kind, a relatively large (100 ± 25 km) divergent sinistral motion until 57 Ma is followed by 90 ± 12 km more of near strait-parallel motion until 54 Ma. The divergent components of the pre-57 Ma motions are confidently defined at 95% level, and fully consistent with the evidence for alkaline volcanism and pull apart basins along the strait (*Estrada et al.*, 2009; *Ehrhardt et al.*, 2016). Allowing inter-block sinistral slip in Ellesmere Island thus offers a plausible resolution to the Wegener Fault debate, as suggested previously (e.g., *Kerr*, 1980; *de Paor et al.*, 1989, and references therein).

5.4.2 The Eurekan Orogen

The eastern Canadian Arctic archipelago presents widespread evidence for Paleocene crustal shortening in the form of multliple fault zones with complex motion histories including thrust and reverse movements (*Piepjohn et al.*, 2016; *Piepjohn and von Gosen*, 2018). The complexity is partially attributable to the fact that many of the structures appear to have originated in the earlier (Paleozoic) Ellesmerian or Innuitian orogeny. A relatively small set of strain estimates, ranging between 100 km of north-south shortening in northwestern Ellesmere Island and 15 km of east-west shortening in Axel Heiberg Island, have been published based on studies of some of these structures (*Harrison*, 2004; *Harrison and Jackson*, 2008; *Harrison*, 2009; *Harrison and Jackson*, 2014). *Gion et al.* (2017) took four of these estimates, from fault systems on Ellesmere and Axel Heiberg islands, as constraints on their plate model. The model's representation of shortening across these four fault systems exceeds the field-estimated total by around 25-65 km. Its authors suggested this not to be significant at the scale of likely observational and interpretational errors. Figure 15 compares *Gion et al.*'s (2017) model to ours in Ellesmere Island. In our model, total shortening across the island, measured north-south, amounts to around 360 km, or 39% of its length before shortening. In *Gion et al.*'s (2017) model, the corresponding figure is 120 km (17%), but this increases to 355 km (38%) if the unconstrained shortening across Nares Strait (Figure 14) is taken into consideration as well.

Beyond the small set of structural studies that deliver numerical shortening estimates, other authors describe how mapped geological structures from the eastern Canadian Arctic islands are consistent with the idea that Paleocene plate convergence with northern Greenland may have occurred in two phases (Figures 2 and 15) (*Tessensohn and Piepjohn*, 2000; *Piepjohn et al.*, 2016). The first phase involved sinistral strike-slip tectonics on faults in eastern and southern Ellesmere Island. The second saw shortening by movements on thrust and reverse faults on both Ellesmere and Axel Heiberg islands, and was accompanied by dextral strike-slip along faults further northwest. Based on examination of *Oakey and Chalmers*' (2012) plate motion model, *Piepjohn et al.* (2016) suggested the change between the two phases occurred at 47 Ma.

Our model is intended to represent the evolution of strain sense and azimuth in field-based structural records taken from large faults of the Eurekan orogeny, rather than to precisely reproduce throw estimates from them. Accordingly, for large fault zones in Ellesmere Island, it portrays early (pre-54 Ma) sinistral transpression and strike-slip on faults that are linked to those in Nares Strait, followed by 120 ± 12 km orthogonal crustal shortening until 49 Ma, dextral oblique convergence (100 ± 7 km) until 40 Ma, and finally dextral strike-slip (55 ± 5 km) (Figure 15). The strain evolution is thus a more gradual rotation than the epochal switch from strike-slip to convergence at ∼47 Ma, as suggested by *Piepjohn et al.* (2016) on the basis of *Oakey and Chalmers*' (2012) GRN-NAM rotations. This contrast is a direct consequence of our GRN-NAM rotation model history's broader U-shaped progression of finite rotation poles and finer resolution than seen in previous models (Figure 8).

6 Conclusions

A set of new plate kinematic models is generated and manipulated to provide a high-resolution context within which to interpret the history of plate motions accommodated in the Labrador Sea, Davis Strait, Baffin Bay, Nares Strait and Eurekan Orogen. The conjugate continental shelf edges of the Labrador Sea separated at 91-88 Ma. Separation started as the plate boundary focussed and propagated northward into a zone of slight and distributed extension that had been active for much or all of the Cretaceous. Propagation was not smooth. The tip of the focussed boundary apparently stalled at the northern end of the Labrador Sea for around 20 Myr until propagating further through Davis Strait and Baffin Bay at ∼69-65 Ma. Propagation appears not to have accompanied any major change in plate divergence rate or azimuth, and may instead have occurred in response to the availability of Iceland plume related melt for focussing the plate boundary in Baffin Bay. In the Labrador Sea, continued plate divergence led to the formation of broad COTZs until, at ∼61 Ma, the onset of NE-SW-oriented oceanic accretion at a stable mid-ocean ridge. Soon after its formation, the ridge was adopted as the site of NNW-SSE-oriented NAM-GRN divergence. The ridge retained its orientation in spite of a large counterclockwise change in plate divergence azimuth. Long (50-90 km) normal faults along the median valley may have started to act in oblique slip, a mode of response that is unknown from presently active mid ocean ridge segments of similar length.

In the Davis Strait, a narrow corridor of transitional and/or oceanic crust would have been generated in pre-Eocene times. Its formation ended as the azimuth of relative plate motion rotated, forcing the plate boundary in the strait into NW-SE oriented plate convergence after 49.34 Ma, generating observed transpressional and compressional structures (*Gregersen et al.*, 2013). In Baffin Bay, Paleocene to Eocene plate divergence (∼64-40.15 Ma) gradually gave way to compression in the north, which has previously been related to the Eurekan Orogen, and lasted until 33.16 Ma at the latest. Slightly further north, our model confidently resolves a detailed history of strike-slip and transtensional faulting along Nares Strait followed by a multi-stage Eurekan Orogeny, together describing a horseshoe-shaped strain evolution path expressed by sinistral transpression, orthogonal convergence, dextral oblique convergence and dextral strike-slip, all of which are independently interpretable from field observations in Ellesmere and Axel Heiberg islands (*Piepjohn et al.*, 2013, 2016).

Acknowledgements

We thank the COMPASS Consortium, Royal Holloway University of London for funding support. We also thank the editors at Tektonika, namely Maëlis Arnould and Mohamed Gouiza, as well as the reviewers for their fair and constructive review of our paper. Figures were produced using the Generic Mapping Tools (GMT *Wessel and Smith*, 1991).

Author contributions

AC and **GE** built the plate kinematic models and drafted the original manuscript and figures, with supporting contributions from **JA** and **LPD** to further refine the original manuscript. Further revisions of the manuscript were undertaken by **AC** and **GE** during the review process.

Data availability

Magnetic data for this paper were obtained from the Global Seafloor Fabric and Magnetic Lineation Data Base Project (*Seton et al.*, 2014). High resolution gravity data (free-air) up to 80°N was obtained from *Sandwell et al.* (2014), and ship-borne gravity data from 80°-90°N were obtained from the Circum-Arctic mapping project (*Gaina et al.*, 2011).
GPlates project control files can be found in supplementary material.

Competing interests

The authors declare no competing interests.

Peer review

This publication was peer-reviewed by Kim Welford, Carmen Gaina, and Simon Williams. The full peer-review report can be found here: Review Report.

Copyright notice

References

Abdelmalak, M. M., S. Planke, S. Polteau, E. H. Hartz, J. I. Faleide, C. Tegner, D. A. Jerram, J. M. Millett, and R. Myklebust (2019), Breakup volcanism and plate tectonics in the NW Atlantic, *Tectonophysics*, *760*, 267–296, doi: 10.1016/j.tecto.2018.08.002.

Altenbernd, T., W. Jokat, I. Heyde, and V. Damm (2014), A crustal model for northern Melville Bay, Baffin Bay, *Journal of Geophysical Research: Solid Earth*, *119*, 8610–8632, doi: 10.1002/2014JB011559.

Barnett-Moore, N., M. Hosseinpour, and S. Maus (2016), Assessing discrepancies between previous plate kinematic models of Mesozoic Iberia and their constraints, *Tectonics*, *35*(8), 1843–1862, doi: 10.1002/2015tc004019.

Bird, P. (2003), An updated digital model of plate boundaries, *Geochemistry, Geophysics, Geosystems*, *4*, doi: 10.1029/2001GC000252.

Brune, S., S. E. Williams, N. P. Butterworth, and R. D. Müller (2016), Abrupt plate accelerations shape rifted continental margins, *Nature*, *536*(7615), 201–204, doi: 10.1038/nature18319.

Chalmers, J. A. (1991), New evidence on the structure of the Labrador Sea/Greenland continental margin, *Journal of the Geological Society*, *148*(5), 899–908, doi: 10.1144/gsjgs.148.5.0899.

Chalmers, J. A., and K. H. Laursen (1995), Labrador Sea: the extent of continental and oceanic crust and the timing of the onset of seafloor spreading, *Marine and petroleum geology*, *12*(2), 205–217, doi: 10.1016/0264-8172(95)92840-s.

Chalmers, J. A., and G. N. Oakey (2007), Cretaceous - Palaeogene development of the Labrador Sea and Davis Strait, in *EGU General Assembly 2007*.

Chalmers, J. A., and T. C. R. Pulvertaft (2001), Development of the continental margins of the Labrador Sea: A review, *Geological Society special publication*, *187*, 77–105, doi: 10.1144/GSL.SP.2001.187.01.05.

Chenin, P., G. Manatschal, S. Picazo, O. Müntener, G. Karner, C. Johnson, and M. Ulrich (2017), Influence of the architecture of magma-poor hyperextended rifted margins on orogens produced by the closure of narrow versus wide oceans, *Geosphere*, *13*, 559–576, doi: 10.1130/GES01363.1.

Chenin, P., S. M. Schmalholz, G. Manatschal, and G. D. Karner (2018), Necking of the lithosphere: A reappraisal of basic concepts with Thermo-mechanical numerical modeling, *Journal of geophysical research. Solid earth*, *123*(6), 5279–5299, doi: 10.1029/2017jb014155.

Chian, D., K. E. Louden, and I. Reid (1995), Crustal structure of the Labrador Sea conjugate margin and implications for the formation of nonvolcanic continental margins, *Journal of Geophysical Research: Solid Earth*, *100*, 24,239–24,253, doi: 10.1029/95JB02162.

Clarke, D. B., and E. K. Beutel (2020), Davis Strait Paleocene picrites: Products of a plume or plates?, *Earth-science reviews*, *206*(102770), 102,770, doi: 10.1016/j.earscirev.2019.01.012.

Cox, A., and R. B. Hart (1991), *Plate tectonics: How it works*, vol. 1, 1 ed., John Wiley & Sons.

Dalhoff, F., L. M. Larsen, J. R. Ineson, S. Stouge, J. A. Bojesen-Koefoed, S. Lassen, A. Kuijpers, J. A. Rasmussen, and H. Nøhr-Hansen (2006), Continental crust in the Davis Strait: new evidence from seabed sampling, *Geological Survey of Denmark and Greenland bulletin*, *10*, 33–36, doi: 10.34194/geusb.v10.4901.

Dawes, P. R., and J. W. Kerr (1982), The case against major displacement along Nares Strait, *Meddelelser om Grønland. Geoscience*, *8*, 369–386, doi: 10.7146/moggeosci.v8i.139614.

de Paor, D. G., D. C. Bradley, G. Eisenstadt, and S. M. Phillips (1989), The Arctic Eurekan orogen: A most unusual fold-and-thrust belt, *Geological Society of America bulletin*, *101*(7), 952–967, doi: 10.1130/0016-7606(1989)101<0952:taeoam>2.3.co;2.

Delescluse, M., T. Funck, S. A. Dehler, K. E. Louden, and L. Watremez (2015), The oceanic crustal structure at the extinct, slow to ultraslow Labrador Sea spreading center, *Journal of geophysical research. Solid earth*, *120*, 5249–5272, doi: 10.1002/2014JB011739.

Dick, H. J. B., J. Lin, and H. Schouten (2003), An ultraslow-spreading class of ocean ridge, *Nature*, *426*(6965), 405–412, doi: 10.1038/nature02128.

Dickie, K., C. E. Keen, G. L. Williams, and S. A. Dehler (2011), Tectonostratigraphic evolution of the Labrador margin, Atlantic Canada, *Marine and petroleum geology*, *28*(9), 1663–1675, doi: 10.1016/j.marpetgeo.2011.05.009.

Døssing, A., and T. Funck (2012), Greenland Fracture Zone–East Greenland Ridge(s) revisited: Indications of a C22-change in plate motion?, doi: 10.1029/2011JB008393.

Døssing, A., J. R. Hopper, A. V. Olesen, T. M. Rasmussen, and J. Halpenny (2013), New aero-gravity results from the Arctic: Linking the latest Cretaceous-early Cenozoic plate kinematics of the North Atlantic and Arctic Ocean, doi: 10.1002/ggge.20253.

Eagles, G. (2004), Tectonic evolution of the Antarctic–Phoenix plate system since 15 Ma, *Earth and planetary science letters*, *217*(1-2), 97–109, doi: 10.1016/s0012-821x(03)00584-3.

Eagles, G. (2019), A little spin in the Indian Ocean plate circuit, *Tectonophysics*, *754*, 80–100, doi: 10.1016/j.tecto.2019.01.015.

Eagles, G. (2024), Overture for the Mandara and Vasuki Plates, *Tektonika*, *2*(1), doi: 10.55575/tektonika2024.2.1.61.

Eagles, G., L. Pérez-Díaz, and N. Scarselli (2015), Getting over continent ocean boundaries, *Earth-science reviews*, *151*, 244–265, doi: 10.1016/j.earscirev.2015.10.009.

Ehrhardt, A., M. Schnabel, V. Damm, and K. Piepjohn (2016), Imaging the plate boundary between Greenland and North America within the Kane Basin by means of geophysical data, *Geophysical research letters*, *43*, 7913–7920, doi: 10.1002/2016GL069329.

Estrada, S., F. Henjes-Kunst, F. Melcher, and F. Tessensohn (2009), Paleocene alkaline volcanism in the Nares Strait region: Evidence from volcanic pebbles, *International journal of earth sciences*, *99*, 863–890, doi: 10.1007/s00531-009-0432-6.

Farangitakis, G. P., P. J. Heron, K. J. W. McCaffrey, J. van Hunen, and L. M. Kalnins (2020), The impact of oblique inheritance and changes in relative plate motion on the development of rift-transform systems, *Earth and planetary science letters*, *541*(116277), 116,277, doi: 10.1016/j.epsl.2020.116277.

Fournier, M., and C. Petit (2007), Oblique rifting at oceanic ridges: Relationship between spreading and stretching directions from earthquake focal mechanisms, *Journal of structural geology*, *29*(2), 201–208, doi: 10.1016/j.jsg.2006.07.017.

Funck, T., H. R. Jackson, K. E. Louden, and F. Klingelhöfer (2007), Seismic study of the transform-rifted margin in Davis Strait between Baffin Island (Canada) and Greenland: What happens when a plume meets a transform, *Journal of geophysical research. Solid earth*, *112*, 1–22, doi: 10.1029/2006JB004308.

Funck, T., K. Gohl, V. Damm, and I. Heyde (2012), Tectonic evolution of southern Baffin Bay and Davis Strait: Results from a seismic refraction transect between Canada and Greenland, *Journal of geophysical research. Solid earth*, *117*, 1–24, doi: 10.1029/2011JB009110.

Gaina, C., W. R. Roest, and R. D. Müller (2002), Late Cretaceous–Cenozoic deformation of northeast Asia, *Earth and planetary science letters*, *197*(3-4), 273–286, doi: 10.1016/s0012-821x(02)00499-5.

Gaina, C., L. Gernigon, and P. Ball (2009), Palaeocene–Recent plate boundaries in the NE Atlantic and the formation of the Jan Mayen microcontinent, *Journal of the Geological Society*, *166*, 601–616, doi: 10.1144/0016-76492008-112.

Gaina, C., S. Werner, R. Saltus, and S. Maus (2011), Circum-Arctic mapping project: New magnetic and gravity anomaly maps of the Arctic, *Geological Society London Memoirs*, *35*, 39–48, doi: 10.1144/M35.3.

Gaina, C., A. Nasuti, G. S. Kimbell, and A. Blischke (2017), Break-up and seafloor spreading domains in the NE Atlantic, *Geological Society special publication*, *447*(1), 393–417, doi: 10.1144/sp447.12.

Geissler, W. H., C. Gaina, J. R. Hopper, T. Funck, A. Blischke, U. Arting, á, G. Péron-Pinvidic, and M. M. Abdelmalak (2017), Seismic volcanostratigraphy of the NE Greenland continental margin, *Geological Society special publication*, *447*(1), 149–170, doi: 10.1144/sp447.11.

Gillard, M., G. Manatschal, and J. Autin (2016), How can asymmetric detachment faults generate symmetric Ocean Continent Transitions?, *Terra nova*, *28*(1), 27–34, doi: 10.1111/ter.12183.

Gilotti, J. A., W. C. McClelland, K. Piepjohn, and W. von Gosen (2018), U–Pb geochronology of Paleoproterozoic gneiss from southeastern Ellesmere Island: implications for displacement estimates on the Wegener fault, *arktos*, *4*(1), 1–18, doi: 10.1007/s41063-018-0047-x.

Gion, A. M., S. E. Williams, and R. D. Müller (2017), A reconstruction of the Eurekan Orogeny incorporating deformation constraints: A Reconstruction of the Eurekan Orogeny Incorporating Deformation Constraints, *Tectonics*, *36*(2), 304–320, doi: 10.1002/2015tc004094.

Goff, J. A. (2023), Regional Variations in the Spreading-Rate Dependence of Abyssal Hill Roughness as Indicators of Mantle Heterogeneity, *Geophysical research letters*, *50*, e2023GL102,801, doi: 10.1029/2023GL102801.

Gradstein, F. M., J. G. Ogg, M. D. Schmitz, and G. M. Ogg (Eds.) (2012), *The geologic time scale 2012*, vol. 2, 1 ed., Elsevier, Oxford, New Zealand, doi: 10.1016/c2011-1-08249-8.

Graham, D. W., L. M. Larsen, B. B. Hanan, M. Storey, A. K. Pedersen, and J. E. Lupton (1998), Helium isotope composition of the early Iceland mantle plume inferred from the Tertiary picrites of West Greenland, *Earth and planetary science letters*, *160*(3-4), 241–255, doi: 10.1016/s0012-821x(98)00083-1.

Gregersen, U., and T. Bidstrup (2008), Structures and hydrocarbon prospectivity in the northern Davis Strait area, offshore West Greenland, *Petroleum geoscience*, *14*(2), 151–166, doi: 10.1144/1354-079308-752.

Gregersen, U., J. R. Hopper, and P. C. Knutz (2013), Basin seismic stratigraphy and aspects of prospectivity in the NE Baffin Bay, Northwest Greenland, *Marine and petroleum geology*, *46*, 1–18, doi: 10.1016/j.marpetgeo.2013.05.013.

Harrison, C. J. (2004), In search of the Wegener Fault: Re-evaluation of strike-slip displacements along and bordering Nares Strait, *Polarforschung*, *74*, 129–160, doi: 10013/epic.29929.d001.

Harrison, J. C. (2009), Regional variation in structural style, deformation kinematics, and summary of tectonic history, northeast Ellesmere Island, *Tech. rep.*, Natural Resources Canada, doi: 10.4095/289649.

Harrison, J. C., and M. P. Jackson (2008), Bedrock geology, Strand Fiord-Expedition Fiord area, western Axel Heiberg Island, northern Nunavut (parts of NTS 59E, F, G, and H), *Tech. rep.*, Natural Resources Canada, doi: 10.4095/225734.

Harrison, J. C., and M. P. A. Jackson (2014), Exposed evaporite diapirs and minibasins above a canopy in central Sverdrup Basin, Axel Heiberg Island, Arctic Canada, *Basin research*, *26*(4), 567–596, doi: 10.1111/bre.12037.

Harrison, J. C., T. A. Brent, and G. N. Oakey (2006), Bedrock geology of the Nares Strait region of Arctic Canada and Greenland with explanatory text and GIS content, *Tech. rep.*, Natural Resources Canada, doi: 10.4095/222524.

Harrison, J. C., T. A. Brent, and G. N. Oakey (2011), Chapter 40: Baffin Fan and its inverted rift system of Arctic eastern Canada: Stratigraphy, tectonics and petroleum resource potential, *Geological Society London Memoirs*, *35*, 595–626, doi: 10.1144/M35.40.

Hellinger, S. J. (1981), The uncertainties of finite rotations in plate tectonics, *Journal of geophysical research*, *86*(B10), 9312–9318, doi: 10.1029/jb086ib10p09312.

Hinz, K., H.-U. Schlüter, A. C. Grant, S. P. Srivastava, D. Umpleby, and J. Woodside (1979), Geophysical transects of the Labrador Sea: Labrador to southwest Greenland, *Tectonophysics*, *59*, 151–183, doi: 10.1016/0040-1951(79)90043-X.

Hopper, J. R., T. Funck, B. E. Tucholke, H. C. Larsen, W. S. Holbrook, K. E. Louden, D. Shillington, and H. Lau (2004), Continental break-up and the onset of ultraslow seafloor spreading off Flemish Cap on the Newfoundland rifted margin, *Geology*, *32*, 93–96, doi: 10.1130/G19694.1.

Hosseinpour, M., R. D. Müller, S. E. Williams, and J. M. Whittaker (2013), Full-fit reconstruction of the Labrador Sea and Baffin Bay, *Solid earth*, *4*(2), 461–479, doi: 10.5194/se-4-461-2013.

Jagoutz, O., O. Müntener, G. Manatschal, D. Rubatto, G. Péron-Pinvidic, B. D. Turrin, and I. M. Villa (2007), The rift-to-drift transition in the North Altantic: A stuttering start of the MORB machine?, *Geology*, *35*, 1087–1090, doi: 10.1130/G23613A.1.

Japsen, P., P. F. Green, and J. A. Chalmers (2023), Synchronous exhumation episodes across Arctic Canada, North Greenland and Svalbard in relation to the Eurekan Orogeny, *Gondwana research: international geoscience journal*, *117*, 207–229, doi: 10.1016/j.gr.2023.01.011.

Keen, C. E., and D. L. Barrett (1972), Seismic Refraction Studies in Baffin Bay: An Example of a Developing Ocean Basin, *Geophysical journal international*, *30*, 253–271, doi: 10.1111/j.1365-246X.1972.tb05812.x.

Keen, C. E., M. J. Keen, D. I. Ross, and M. Lack (1974), Baffin bay: Small ocean basin formed by sea-floor spreading, *AAPG bulletin*, *58*, 1089–1108, doi: 10.1306/83d91619-16c7-11d7-8645000102c1865d.

Keen, C. E., K. Dickie, and L. T. Dafoe (2018), Structural characteristics of the ocean-continent transition along the rifted continental margin, offshore central Labrador, *Marine and petroleum geology*, *89*, 443–463, doi: 10.1016/j.marpetgeo.2017.10.012.

Kerr, J. W. (1980), A plate tectonic contest in Arctic Canada, Geological Survey of Canada.

Klitgord, K. D., and H. Schouten (1986), Plate kinematics of the central Atlantic, in *The Western North Atlantic Region*, pp. 351–378, Geology of North America, North America, doi: 10.1130/dnag-gna-m.351.

Knudsen, C., U. Gregersen, T. F. Kokfelt, M. Olivarius, and T. B. Thomsen (2020), A mid-Cretaceous alkaline volcano in the Davis Strait, *Canadian journal of earth sciences*, *57*, 69–86, doi: 10.1139/cjes-2018-0307.

Knutz, C. P., G. U. Gregersen, and R. J. Hopper (2012), Late Paleogene submarine fans in Baffin bay and north-west Greenland, in *74th EAGE Conference and Exhibition incorporating EUROPEC 2012*, EAGE Publications BV, Netherlands, doi: 10.3997/2214-4609.20148203.

Kristoffersen, Y., and M. Talwani (1977), Extinct triple junction south of Greenland and the Tertiary motion of Greenland relative to North America, *Geological Society of America bulletin*, *88*, 1037–1049, doi: 10.1130/0016-7606(1977)88<1037:ETJSOG>2.0.CO;2.

Larsen, H. C., and A. D. Saunders (1998), Tectonism and volcanism at the southeast Greenland rifted margin: a record of plume impact and later continental rupture, in *Proceedings of the Ocean Drilling Program*, vol. 152, pp. 503–533, Ocean Drilling Program, doi: 10.2973/odp.proc.sr.152.240.1998.

Larsen, L. M., and M.-C. Williamson (2020), Depleted and ultradepleted basalt and picrite in the Davis Strait: Paleocene volcanism associated with a transform continental margin, *Geological magazine*, *157*(12), 1983–2003, doi: 10.1017/s0016756820000175.

Larsen, L. M., L. M. Heaman, R. A. Creaser, R. A. Duncan, R. Frei, and M. Hutchison (2009), Tectonomagmatic events during stretching and basin formation in the Labrador Sea and the Davis Strait: evidence from age and composition of Mesozoic to Palaeogene dyke swarms in West Greenland, *Journal of the Geological Society*, *166*(6), 999–1012, doi: 10.1144/0016-76492009-038.

Lawver, L. A., R. D. Müller, S. P. Srivastava, and W. Roest (1990), The opening of the arctic ocean, in *Geological History of the Polar Oceans: Arctic versus Antarctic*, pp. 29–62, Springer Netherlands, Dordrecht, doi: 10.1007/978-94-009-2029-3_3.

Livermore, R., A. Nankivell, G. Eagles, and P. Morris (2005), Paleogene opening of Drake passage, *Earth and planetary science letters*, *236*(1-2), 459–470, doi: 10.1016/j.epsl.2005.03.027.

Longley, L., J. Phethean, and C. Schiffer (2024), The Davis Strait proto-microcontinent: The role of plate tectonic reorganization in continental cleaving, *Gondwana research: international geoscience journal*, *133*, 14–29, doi: 10.1016/j.gr.2024.05.001.

MacLeod, S. J., S. E. Williams, K. J. Matthews, R. D. Müller, and X. Qin (2017), A global review and digital database of large-scale extinct spreading centers, *Geosphere*, *13*, 911–949, doi: 10.1130/GES01379.1.

Macnab, R., J. Verhoef, W. Roest, and J. Arkani-Hamed (1995), New database documents the magnetic character of the Arctic and North Atlantic, *Eos*, *76*, 449–458, doi: 10.1029/95EO00278.

Matthews, K. J., K. T. Maloney, S. Zahirovic, S. E. Williams, M. Seton, and R. D. Müller (2016), Global plate boundary evolution and kinematics since the late Paleozoic, *Global and planetary change*, *146*, 226–250, doi: 10.1016/j.gloplacha.2016.10.002.

Merkouriev, S., and C. DeMets (2008), A high-resolution model for Eurasia-North America plate kinematics since 20 Ma, *Geophysical journal international*, *173*(3), 1064–1083, doi: 10.1111/j.1365-246x.2008.03761.x.

Müller, R. D., M. Sdrolias, C. Gaina, and W. R. Roest (2008), Age, spreading rates, and spreading asymmetry of the world's ocean crust, *Geochemistry, Geophysics, Geosystems*, *9*, 1–19, doi: 10.1029/2007GC001743.

Müller, R. D., S. Zahirovic, S. E. Williams, J. Cannon, M. Seton, D. J. Bower, M. G. Tetley, C. Heine, E. Le Breton, S. Liu, S. H. J. Russell, T. Yang, J. Leonard, and M. Gurnis (2019), A Global Plate Model Including Lithospheric Deformation Along Major Rifts and Orogens Since the Triassic, *Tectonics*, *38*(6), 1884–1907, doi: 10.1029/2018TC005462.

Nankivell, A. (1997), Tectonic evolution of the Southern Ocean between Antarctica, South America and Africa over the past 84Ma, *PhD thesis*.

NOAA National Geophysical Data Center (2023), Marine Trackline Geophysical Database, doi: 10.7289/V5CZ35DR.

Nøhr-Hansen, H. (2003), Dinoflagellate cyst stratigraphy of the Palaeogene strata from the Hellefisk-1, Ikermiut-1, Kangâmiut-1, Nukik-1, Nukik-2 and Qulleq-1 wells, offshore West Greenland, *Marine and petroleum geology*, *20*(9), 987–1016, doi: 10.1016/s0264-8172(02)00116-2.

Oakey, G. N. (2005), Cenozoic evolution and lithosphere dynamics of the Baffin Bay – Nares Strait region of Arctic Canada and Greenland, Ph.D. thesis, Vrije Universiteit Amsterdam, Amsterdam, Netherlands.

Oakey, G. N., and J. A. Chalmers (2012), A new model for the Paleogene motion of Greenland relative to North America: Plate reconstructions of the Davis Strait and Nares Strait regions between Canada and Greenland, *Journal of Geophysical Research, [Solid Earth]*, *117*(B10), doi: 10.1029/2011JB008942.

Oakey, G. N., and R. Stephenson (2008), Crustal structure of the Innuitian region of Arctic Canada and Greenland from gravity modelling: Implications for the Palaeogene Eurekan orogen, *Geophysical journal international*, *173*, 1039–1063, doi: 10.1111/j.1365-246X.2008.03784.x.

Paige, C. C., and M. A. Saunders (1982), LSQR, An algorithm for sparse linear equations and sparse least squares, *ACM Trans. Math. Software*, *8*, 43–71.

Peace, A., K. McCaffrey, J. Imber, J. Phethean, G. Nowell, K. Gerdes, and E. Dempsey (2016), An evaluation of Mesozoic rift-related magmatism on the margins of the Labrador Sea: Implications for rifting and passive margin asymmetry, *Geosphere*, *12*, 1701–1724, doi: 10.1130/GES01341.1.

Peace, A., K. McCaffrey, J. Imber, J. van Hunen, R. Hobbs, and R. Wilson (2018), The role of pre-existing structures during rifting, continental breakup and transform system development, offshore West Greenland, *Basin research*, *30*(3), 373–394, doi: 10.1111/bre.12257.

Peace, A. L., G. R. Foulger, C. Schiffer, and K. J. W. McCaffrey (2017), Evolution of Labrador Sea–Baffin Bay: Plate or plume processes?, *Geoscience Canada*, *44*(3), 91–102, doi: 10.12789/geocanj.2017.44.120.

Piepjohn, K., and W. von Gosen (2018), Structural transect through Ellesmere Island (Canadian Arctic): superimposed Palaeozoic Ellesmerian and Cenozoic Eurekan deformation, *Geological Society special publication*, *460*(1), 33–56, doi: 10.1144/sp460.5.

Piepjohn, K., W. von Gosen, A. Läufer, W. C. McClelland, and S. Estrada (2013), Ellesmerian and Eurekan fault tectonics at the northern margin of Ellesmere Island (Canadian High Arctic) [Ellesmerische und Eurekan-Störungstektonik am Nordrand von Ellesmere Island (kanadische Hocharktis).], *Zeitschrift der Deutschen Gesellschaft für Geowissenschaften*, *164*(1), 81–105, doi: 10.1127/1860-1804/2013/0007.

Piepjohn, K., W. von Gosen, and F. Tessensohn (2016), The Eurekan deformation in the Arctic: an outline, *Journal of the Geological Society*, *173*(6), 1007–1024, doi: 10.1144/jgs2016-081.

Pérez-Díaz, L., G. Eagles, and K. Sigloch (2020), Indo-Atlantic plate accelerations around the Cretaceous-Paleogene boundary: A time-scale error, not a plume-push signal, *Geology*, *48*(12), 1169–1173, doi: 10.1130/g47859.1.

Pérez-Gussinyé, M., and T. J. Reston (2001), Rheological evolution during extension at nonvolcanic rifted margins: Onset of serpentinization and development of detachments leading to continental breakup, doi: 10.1029/2000JB900325.

Rasmussen, T. M., and P. R. Dawes (2011), Kennedy Channel and its geophysical lineaments: new evidence that the Wegener Fault is a myth, *Geological Survey of Denmark and Greenland bulletin*, *23*, 69–72, doi: 10.34194/geusb.v23.4875.

Reid, I., and H. R. Jackson (1997), Crustal structure of northern Baffin Bay: Seismic refraction results and tectonic implications, *Journal of geophysical research*, *102*(B1), 523–542, doi: 10.1029/96jb02656.

Roest, W. R., and S. P. Srivastava (1989), Sea-floor spreading in the Labrador Sea: a new reconstruction, *Geology*, *17*, 1000–1003, doi: 10.1130/0091-7613(1989)017<1000:SFSITL>2.3.CO;2.

Roest, W. R., and S. P. Srivastava (1991), Kinematics of the plate boundaries between Eurasia, Iberia, and Africa in the North Atlantic from the Late Cretaceous to the present, *Geology*, *19*, 613–616, doi: 10.1130/0091-7613(1991)019<0613:KOTPBB>2.3.CO;2.

Saalmann, K., F. Tessensohn, K. Piepjohn, W. von Gosen, and U. Mayr (2005), Structure of Palaeogene sediments in east Ellesmere Island: Constraints on Eurekan tectonic evolution and implications for the Nares Strait problem, *Tectonophysics*, *406*(1-2), 81–113, doi: 10.1016/j.tecto.2005.06.005.

Sandwell, D. T., R. D. Müller, W. H. F. Smith, E. Garcia, and R. Francis (2014), Marine geophysics. New global marine gravity model from CryoSat-2 and Jason-1 reveals buried tectonic structure, *Science (New York, N.Y.)*, *346*(6205), 65–67, doi: 10.1126/science.1258213.

Schouten, T., and D. van Hinsbergen (2021), Deciphering paleogeography from orogenic architecture: constructing orogens by a future closure of the Indian Ocean as thought experiment, in *EGU General Assembly 2021*, Copernicus GmbH, doi: 10.5194/egusphere-egu21-7270.

Seton, M., R. D. Müller, S. Zahirovic, C. Gaina, T. Torsvik, G. Shephard, A. Talsma, M. Gurnis, M. Turner, S. Maus, and M. Chandler (2012), Global continental and ocean basin reconstructions since 200Ma, *Earth-science reviews*, *113*(3-4), 212–270, doi: 10.1016/j.earscirev.2012.03.002.

Seton, M., J. Whittaker, P. Wessel, R. Müller, C. Demets, S. Merkouriev, S. Cande, C. Gaina, G. Eagles, R. Granot, J. Stock, N. Wright, and S. Williams (2014),

Community infrastructure and repository for marine magnetic identifications, *Geochemistry*, *15*, 1629–1641, doi: 10.1002/2013GC005176.

Seton, M., R. D. Müller, S. Zahirovic, S. Williams, N. M. Wright, J. Cannon, J. M. Whittaker, K. J. Matthews, and R. McGirr (2020), A global data set of present-day oceanic crustal age and seafloor spreading parameters, *Geochemistry, geophysics, geosystems: G(3)*, *21*(10), 1–15, doi: 10.1029/2020gc009214.

Shaw, P. R., and S. C. Cande (1990), High-resolution inversion for South Atlantic Plate kinematics using joint altimeter and magnetic anomaly data, *Journal of Geophysical Research: Solid Earth*, *95*, 2625–2644, doi: 10.1029/JB095iB03p02625.

Sibuet, J.-C., S. Srivastava, and G. Manatschal (2007), Exhumed mantle-forming transitional crust in the Newfoundland-Iberia rift and associated magnetic anomalies, *Journal of Geophysical Research: Solid Earth*, *112*, doi: 10.1029/2005JB003856.

Srivastava, S. P. (1978), Evolution of the Labrador Sea and its bearing on the early evolution of the North Atlantic, *Geophysical journal international*, *52*, 313–357, doi: 10.1111/j.1365-246X.1978.tb04235.x.

Srivastava, S. P. (1983), Davis strait: Structures, origin and evolution, in *Structure and Development of the Greenland-Scotland Ridge*, vol. 8, edited by T. M. Thiede J. Bott M.H.P., pp. 159–189, Springer US, Boston, MA, doi: 10.1007/978-1-4613-3485-9_10.

Srivastava, S. P. (1985), Evolution of the Eurasian Basin and its implications to the motion of Greenland along Nares Strait, *Tectonophysics*, *114*(1-4), 29–53, doi: 10.1016/0040-1951(85)90006-x.

Srivastava, S. P., and C. E. Keen (1995), A deep seismic reflection profile across the extinct Mid-Labrador Sea spreading center, *Tectonics*, *14*(2), 372–389, doi: 10.1029/94tc02453.

Srivastava, S. P., and W. R. Roest (1999), Extent of oceanic crust in the Labrador Sea1, *Marine and petroleum geology*, *16*(1), 65–84, doi: 10.1016/s0264-8172(98)00041-5.

Srivastava, S. P., and C. R. Tapscott (1986), Plate kinematics of the North Atlantic, in *The Western North Atlantic Region*, vol. M, pp. 379–404, Geology of North America, North America, doi: 10.1130/dnag-gna-m.379.

Stanton, N., G. Manatschal, J. Autin, D. Sauter, M. Maia, and A. Viana (2016), Geophysical fingerprints of hyper-extended, exhumed and embryonic oceanic domains: the example from the Iberia–Newfoundland rifted margins, *Marine Geophysical Research*, *37*(3), 185–205, doi: 10.1007/s11001-016-9277-0.

Suckro, S. K., K. Gohl, T. Funck, I. Heyde, A. Ehrhardt, B. Schreckenberger, J. Gerlings, V. Damm, and W. Jokat (2012), The crustal structure of southern Baffin Bay: Implications from a seismic refraction experiment, *Geophysical journal international*, *190*, 37–58, doi: 10.1111/j.1365-246X.2012.05477.x.

Sørensen, E. V., J. R. Hopper, G. K. Pedersen, H. Nøhr-Hansen, P. Guarnieri, A. K. Pedersen, and F. G. Christiansen (2017), Inversion structures as potential petroleum exploration targets on Nuussuaq and northern Disko, onshore West Greenland, *Geological Survey of Denmark and Greenland bulletin*, *38*, 45–48, doi: 10.34194/geusb.v38.4406.

Tappe, S., S. F. Foley, A. Stracke, R. L. Romer, B. A. Kjarsgaard, L. M. Heaman, and N. Joyce (2007), Craton reactivation on the Labrador Sea margins: 40Ar/39Ar age and Sr–Nd–Hf–Pb isotope constraints from alkaline and carbonatite intrusives, *Earth and planetary science letters*, *256*(3-4), 433–454, doi: 10.1016/j.epsl.2007.01.036.

Tegner, C., M. Storey, P. M. Holm, S. B. Thorarinsson, X. Zhao, C.-H. Lo, and M. F. Knudsen (2011), Magmatism and Eurekan deformation in the High Arctic Large Igneous Province: 40Ar–39Ar age of Kap Washington Group volcanics, North Greenland, *Earth and planetary science letters*, *303*(3-4), 203–214, doi: 10.1016/j.epsl.2010.12.047.

Tessensohn, F., and K. Piepjohn (2000), Eocene compressive deformation in Arctic Canada, North Greenland and Svalbard and its plate tectonic causes, *Polarforschung*, *68*, 121–124.

Tessensohn, F., R. H. Jackson, and I. D. Reid (2004), The tectonic evolution of Nares Strait: Implications of new data, *Polarforschung*, *74*, 191–198.

Torsvik, T. H., R. D. Müller, R. V. D. Voo, B. Steinberger, and C. Gaina (2008), Global plate motion frames: Toward a unified model, *Reviews of geophysics (Washington, D.C.: 1985)*, *46*, doi: 10.1029/2007RG000227.

Tucholke, B. E., and A. Virginia (1985), Basement structure and sediment distribution in northwest Atlantic ocean, *AAPG bulletin*, *69*, 2077–2097, doi: 10.1306/948855ed-1704-11d7-8645000102c1865d.

Watts, A. B., and J. D. Fairhead (1999), A process-oriented approach to modeling the gravity signature of continental margins, *Leading Edge*, *18*(2), 258–263, doi: 10.1190/1.1438270.

Welford, J. K., and J. Hall (2013), Lithospheric structure of the Labrador Sea from constrained 3-D gravity inversion, *Geophysical journal international*, *195*(2), 767–784, doi: 10.1093/gji/ggt296.

Welford, J. K., A. L. Peace, M. Geng, S. A. Dehler, and K. Dickie (2018), Crustal structure of Baffin Bay from constrained three-dimensional gravity inversion and deformable plate tectonic models, *Geophysical journal international*, *214*(2), 1281–1300, doi: 10.1093/gji/ggy193.

Wessel, P., and W. H. F. Smith (1991), Free software helps map and display data, *Eos*, *72*(41), 441–446, doi: 10.1029/90eo00319.

Whittaker, J. M., J. C. Afonso, S. Masterton, R. D. Müller, P. Wessel, S. E. Williams, and M. Seton (2015), Long-term interaction between mid-ocean ridges and mantle plumes, *Nature geoscience*, *8*(6), 479–483, doi: 10.1038/ngeo2437.

Whittaker, R. C., and N. E. Hamann (1997), A new frontier province offshore northwest Greenland: Structure, basin development, and petroleum potential of the Melville bay area, *AAPG bulletin*, *81 (1997)*, 978–998, doi: 10.1306/522b49b5-1727-11d7-8645000102c1865d.